

Exploratory MPAS Sensitivity Experiments on Rainforest Biogenic Salt Aerosols, Tropical Rainfall, and Poleward Moisture Transport

AUTHOR

Brian Lue

Independent Researcher

Email: bluesaltbarrier@gmail.com

ORCID: [to be added]

PEER-REVIEW STATUS

This paper is a **non-peer-reviewed preprint submitted to EarthArXiv**. It has not been submitted to a journal for peer review at the time of this preprint release. The author welcomes community feedback, code review, and independent replication.

VERSION 2 — CHANGE NOTES

Version 2 adds the bug-fixed January 120 km paired experiment (Section 6.6) which was completed after v1 submission. Key additions: (i) seasonal mirror partially confirmed — rain redistribution, 30°N transport, 30°S transport, and Antarctic temperature flip sign between April and January exactly as the moisture-barrier hypothesis predicts; (ii) Arctic warming occurs in both seasons and does not mirror, discussed as either a dry-heat pathway, Arctic amplification feedback, or weather noise; (iii) revised Figure 13 (all-phases plot) including the January bug-fix line; (iv) Figures 14 and 15 added for the January 120 km temperature and precipitation maps. Central thesis (biogenic salt is a sensitive variable with ~300 TW of 30°N transport swing across implementations) is strengthened by the seasonal-swing evidence. No changes to methodology, bug-fix history, or conclusions otherwise.

OPEN-RESEARCH MATERIALS

Code and data: github.com/bluesaltbarrier/blue-salt-barrier

Project website: bluesaltbarrier.github.io/blue-salt-barrier

Docker container: ghcr.io/bluesaltbarrier/mpas8-gccn:slim

License: Creative Commons Attribution 4.0 (CC BY 4.0)

CORRESPONDING AUTHOR

Brian Lue — bluesaltbarrier@gmail.com

MASTODON HANDLE FOR EARTHARXIV ANNOUNCEMENT TAGGING

[to be added if author has a Mastodon account]

Exploratory MPAS Sensitivity Experiments on Rainforest Biogenic Salt Aerosols, Tropical Rainfall, and Poleward Moisture Transport

Phase 7 revision: Pöhlker baseline-CCN sensitivity matrix

Brian Lue

Independent Researcher

bluesaltbarrier@gmail.com · ORCID: [to be added] · github.com/bluesaltbarrier/blue-salt-barrier

April 2026

DRAFT PREPRINT — OPEN FOR COMMUNITY REVIEW AND COLLABORATION

ABSTRACT

Rainforest ecosystems emit biologically influenced aerosol particles, including potassium-rich and other hygroscopic components that may affect warm-rain microphysics. While tropical biogenic aerosols have been studied extensively, their sensitivity within coarse-resolution global models remains incompletely characterized, particularly under differing background aerosol states. Here we present exploratory sensitivity experiments using MPAS-Atmosphere to test whether rainforest biogenic salt aerosol parameterizations can alter modeled tropical precipitation and selected large-scale moisture-transport diagnostics.

Using 30-day single-member simulations at 240 km and 120 km resolution, we examined ten alternative implementations ranging from simple autoconversion perturbations to a more explicit giant-cloud-condensation-nuclei (GCCN) lifecycle treatment with activation, condensational growth, coalescence, and wet scavenging. Across these implementations, diagnosed latent heat transport at 30°N varied substantially (range -211 to +153 TW; standard deviation ~126 TW – comparable in magnitude to some published transport estimates), indicating strong sensitivity of some circulation metrics to aerosol microphysical assumptions within these experiments.

A more robust and interpretable result emerged locally: the sign of the modeled Amazon rainfall response depended on baseline aerosol loading. Under a polluted baseline aerosol state (MPAS default, ~4,400 nwfa/cm³), added hygroscopic K-salt particles suppressed local rainfall (-17.1 mm/30-day). Under a pristine low-CCN baseline informed by published Amazon observations (~150 cm⁻³; Pöhlker et al. 2012), the same perturbation enhanced local rainfall (+5.4 to +5.6 mm/30-day). This regime dependence is qualitatively consistent with established aerosol-cloud theory in which precipitation responses vary with background cloud condensation nuclei concentrations.

These simulations are not intended as detection or attribution evidence and are limited by coarse resolution, short integrations, single realizations, and convective parameterization uncertainty. Rather, they demonstrate that rainforest bioaerosol assumptions can materially influence modeled tropical rainfall responses and some transport diagnostics. The results motivate targeted follow-up using convection-permitting ensembles, observational constraints on rainforest aerosol emissions, and higher-fidelity cloud microphysics. We release all code, bug-fix patches, Docker builds, and analysis scripts at github.com/bluesaltbarrier/blue-salt-barrier.

Statistical humility: All simulations reported in this manuscript are single-member 30-day integrations. Any signal smaller than the chaotic variability between two such runs cannot be distinguished from internal noise. No detection or attribution claim is made.

1. Origin of the Hypothesis

1.1 Author Background

The author is an independent researcher with an engineering and numerical-modeling background. This work was conducted outside formal atmospheric-science institutions and is offered as an open, testable hypothesis; domain experts are explicitly invited to improve upon every aspect of it.

1.2 Motivation: Conduction Alone Is Insufficient

Polar ice loss depends on multiple coupled processes beyond simple local conductive exchange, including oceanic, radiative, and atmospheric transport pathways. Earth's atmosphere can be viewed as a heat-redistribution system in which latent heat is released at low latitudes and sensible heat is lost at high latitudes; any mechanism that modulates *where* latent heat is released affects the poleward transport budget. This framing motivates the present investigation of rainforest biogenic aerosols as potential modulators of that budget. The development-history narrative of this work, including multi-year attempts to install WRF and the subsequent AI-assisted computational breakthrough, is disclosed in the Acknowledgments rather than here.

The narrative account of how this hypothesis emerged from informal observation is consolidated in **Appendix B: Origin of the Idea**; it is not required for the scientific content that follows.

2. Introduction

The dominant explanation for polar ice loss centers on radiative forcing from anthropogenic greenhouse gases, primarily CO₂. While this mechanism is well-established, the observed rate of Arctic and Antarctic warming has consistently exceeded model predictions, suggesting additional contributing factors may be missing from current climate models.

We propose one such factor: the loss of biogenic salt aerosol emissions from deforested equatorial rainforests. Pöhlker et al. (2012) demonstrated that fungi associated with Amazon rainforest trees eject potassium salt nanoparticles into the boundary layer, where they serve as seeds for secondary organic aerosol growth and ultimately function as cloud condensation nuclei. We hypothesize that this biological salt emission acts as a **moisture stratification barrier**—a mechanism that traps the atmospheric hydrological cycle at low latitudes, preventing the poleward transport of latent heat.

When this barrier is removed through deforestation, moisture that would have precipitated locally near the equator instead travels poleward, condensing at higher latitudes and releasing its latent heat into the mid-latitude and polar atmosphere (see §3.1). This would represent a direct, non-radiative pathway for redistributing heat that we have not found explicitly isolated as a dedicated process in current mainstream climate-model configurations.

3. The Physical Mechanism

3.1 Latent Heat Transport

Atmospheric energy transport from equator to poles is dominated by latent heat, which accounts for roughly 70% of the total poleward energy flux. When water evaporates at tropical surfaces, it absorbs 2,500 J/g and stores this energy invisibly as latent heat. This energy is released only when the vapor condenses back to liquid—forming clouds and precipitation. The critical question for polar climate is not how much water evaporates, but *where it condenses*.

3.2 Salt as a Moisture Trap

Intact rainforest ecosystems emit highly hygroscopic biogenic salt particles and salt-containing aerosol cores, including the KCl-rich accumulation-mode aerosol population documented by Pöhlker et al. (2012, Fig. S10A) with geometric mean diameter $D_g = 150$ nm ($\sigma_g = 1.43$). Under the high humidity of the tropical boundary layer (>80% RH), these

hygroscopic particles can swell substantially and, once in cloud, may grow by condensation into efficient warm-rain embryos. The observed size distribution spans from nanometer-scale cores to micrometer-scale aged particles; this work focuses on the warm-rain-embryo pathway that becomes active once particles reach collector size. This is the same broad physical mechanism exploited in operational cloud-seeding programs worldwide (Mather et al. 1997, CAIPEEX 2023).

The net effect is that rain forms faster and falls locally, close to the forest that produced the salt. The moisture — and its latent heat — is deposited in the equatorial atmosphere rather than being transported poleward by the Hadley circulation.

3.3 The Critical Distinction: GCCN vs. Small CCN

An important nuance separates this mechanism from the well-studied aerosol indirect effect, which has been examined extensively since Twomey (1977) established the cloud-albedo indirect effect and Albrecht (1989) extended it to cloud-lifetime considerations. Standard small CCN ($<0.2 \mu\text{m}$), such as pollution aerosols, *suppress* rain by creating many small cloud droplets that are inefficient at collision-coalescence (the Twomey effect; further developed in Rosenfeld et al. 2008; Andreae et al. 2004 demonstrated the same pattern in biomass-burning-contaminated Amazon air). Tree-emitted salt particles in the accumulation-mode size range behave differently — as hygroscopic particles that activate at low supersaturation and can initiate warm rain via collision-coalescence once droplets grow past the coalescence gap (traditionally termed **giant CCN (GCCN)** for particles above $\sim 1 \mu\text{m}$; Jensen & Lee 2008). The two regimes have opposite effects on precipitation, and the transition between them depends on the baseline aerosol state (Stevens & Feingold 2009; Koren et al. 2014); this regime dependence is directly relevant to the Phase 7 sign flip reported in §6.9.

PROPERTY	SMALL CCN (POLLUTION)	HYGROSCOPIC SALT (GCCN)
Dry particle size	0.05–0.2 μm	$\sim 150 \text{ nm Dg}$ (Pöhlker 2012, Fig. S10A); grown to collector size in cloud
Effect on rain	Suppressed / delayed	Enhanced / accelerated

PROPERTY	SMALL CCN (POLLUTION)	HYGROSCOPIC SALT (GCCN)
Moisture fate	Stays in cloud longer	Rains out locally
Net transport effect	May increase poleward	Reduces poleward

3.4 Size Optimization and the Accumulation-Mode Peak

Within the accumulation-mode size range (0.1–1 μm) that Pöhlker et al. (2012) observed for pristine Amazon aerosol, activation efficiency is not uniform. Köhler theory predicts that the critical supersaturation (S_{crit}) required to activate a hygroscopic particle as a cloud droplet scales approximately as $d^{-3/2}$ for fixed hygroscopicity κ . The practical consequence is a sharp dependence on diameter:

DRY DIAMETER	K	S_{CRIT}	ACTIVATION IN TYPICAL TROPICAL UPDRAFTS
40 nm	0.4 (sulfate-like)	~0.3–0.5%	Only in vigorous convection
80 nm	0.4	~0.15–0.25%	Often, not reliably
160 nm	0.8 (KCl-like)	~0.03–0.05%	Essentially any updraft

A 160 nm KCl particle activates at roughly one-tenth the supersaturation required for a 40 nm sulfate particle, so it contributes to rain formation across a much wider range of meteorological conditions.

On the activation equation used here. The activation calculation we employ (Petters & Kreidenweis 2007 κ -Köhler; full details in Appendix A.1) is explicitly the neutral form — it contains no charge term, no Coulomb cross-section, no Debye length. This is appropriate because airborne aerosols in the cloud regime are electrically neutral to within small-correction order. The plasma-physics training referenced in §1 (researcher background) enters this work as **shared mathematical structure** — kinetic-theory treatment of

many-particle collisional evolution, activation thresholds, and distribution-function balance — not as literal equation identity. Setting charges to zero in plasma ionization equations (Saha, or kinetic with Coulomb cross-sections) does not recover κ -Köhler; it yields inert neutral particles with no activation. The two physical regimes share a kinetic-theory framework but not governing equations.

Pöhlker et al. (2012, supplementary Fig. S10A) report the pristine Amazon accumulation-mode size distribution as a log-normal with geometric mean diameter **D_g = 150 nm** and $\sigma_g = 1.43$ (Aitken mode at D_g = 67 nm, $\sigma_g = 1.32$ contributes the smaller particles). The ~150 nm accumulation-mode peak coincides with what a physical optimization of (CCN efficiency × atmospheric persistence ÷ emission mass cost) would predict:

- **Sub-100 nm particles** activate only in strong updrafts; in clean air, most never nucleate cloud drops and so do not contribute to rain.
- **Super-micrometer particles** activate reliably but biosynthesis cost scales as diameter-cubed, and gravitational settling shortens their atmospheric lifetime.
- **~150 nm accumulation-mode particles** activate essentially every time cloudy air is lifted, persist ~7 days in the atmosphere (long enough to disperse through the canopy region), and minimize the per-particle biosynthetic cost.

We do not claim this coincidence proves a selective relationship between forest emission chemistry and regional precipitation. The match between the observed peak and the physical efficiency optimum is, however, consistent with co-evolution of rainforest ecosystems and their self-sustaining *local* rain cycle. At minimum it constrains what the representative size should be in any modeling of the K-salt pathway: ~150 nm diameter, not the 80 nm default of the Thompson aerosol-aware microphysics scheme we employ here. In the Phase 7 sensitivity matrix (§6.9), the closest Thompson lookup option to Pöhlker's D_g is 1=4 (80 nm radius = 160 nm diameter). We take this 1=4 configuration as our primary Pöhlker-matched physics, with 1=5 (320 nm diameter) reported as an upper-bound sensitivity test rather than a Pöhlker-matched configuration.

Attribution note. Pöhlker et al. (2012) documented each empirical component drawn on above: the log-normal accumulation-mode size distribution (D_g = 150 nm, $\sigma_g = 1.43$) of pristine Amazon aerosol, the much higher CCN activation efficiency of accumulation-mode particles relative to the Aitken mode (“accumulation mode particles are by orders of magnitude more frequently activated”), and the biological machinery for K-salt emission

(active wet discharge by Ascomycota and Basidiomycota fungi, plant transpiration, guttation, wax abrasion). Pöhlker et al. did not, however, combine these into an explicit evolutionary-optimization or co-evolution argument. The synthesis presented in this section — that the observed accumulation-mode peak size coincides with a tradeoff optimum of (CCN efficiency \times atmospheric persistence \div emission mass cost), consistent with selective co-evolution for local-rainfall fitness — is our own.

4. Experimental Design

4.1 Model Configuration

We used the Model for Prediction Across Scales (MPAS-Atmosphere, version 7.0) with a quasi-uniform 240 km global mesh (10,242 hexagonal Voronoi cells, each with 55 vertical levels stacked from the surface to \sim 30 km altitude, totaling 563,310 computational grid points). The vertical spacing is non-uniform: \sim 50 m layers near the surface to resolve the boundary layer where salt aerosols are emitted and mixed, expanding to \sim 1 km layers in the upper troposphere where dry air is transported poleward. MPAS uses a Voronoi tessellation of the sphere, avoiding the polar singularity and boundary artifacts that affect regional models like WRF when applied to global-scale transport problems.

Physics parameterizations include Thompson microphysics, RRTMG radiation, YSU planetary boundary layer, Noah land surface model, and Kain-Fritsch cumulus convection. Simulations were initialized from GFS analysis data for April 12, 2026 (240 km runs) and January 12, 2025 (120 km seasonal test), each run for 30 days.

A higher-resolution 120 km uniform mesh (40,962 cells, 55 vertical levels, 2.25 million grid points) was used for the Phase 6 seasonal test. This mesh is available from NCAR and is the same Voronoi geometry at $4\times$ the cell count of the 240 km mesh.

4.2 Salt Parameterization

Since MPAS v7.0 does not include explicit GCCN treatment, we parameterized the net effect of hygroscopic salt by enhancing the cloud-to-rain autoconversion rate in the equatorial belt

(10°S–10°N). After each microphysics timestep, an additional fraction of cloud water is converted to rain in equatorial grid cells, representing the accelerated coalescence from GCCN salt particles.

Four enhancement levels were tested in paired simulations against a no-salt baseline:

RUN	ENHANCEMENT	PHYSICAL MEANING
NO-SALT	0%	Complete deforestation, no salt seeding
CONTROL-3	3%	Moderate salt effect
CONTROL-5	5%	Moderate-strong salt effect
CONTROL-25	25%	Strong salt effect (upper bound)

Limitation. This autoconversion parameterization is a first-order approximation. It does not model individual salt particles, their advection by the wind, or their size-dependent activation as CCN. The more physically complete treatment using MPAS v8.3.1 with a dedicated GCCN tracer is described in Section 6.5.

5. Results

5.1 Poleward Latent Heat Transport

The primary diagnostic is the vertically-integrated meridional latent heat flux, computed as $v \times L_v \times q \times dp/g$ and averaged over the 30-day simulation period. Positive values indicate northward transport.

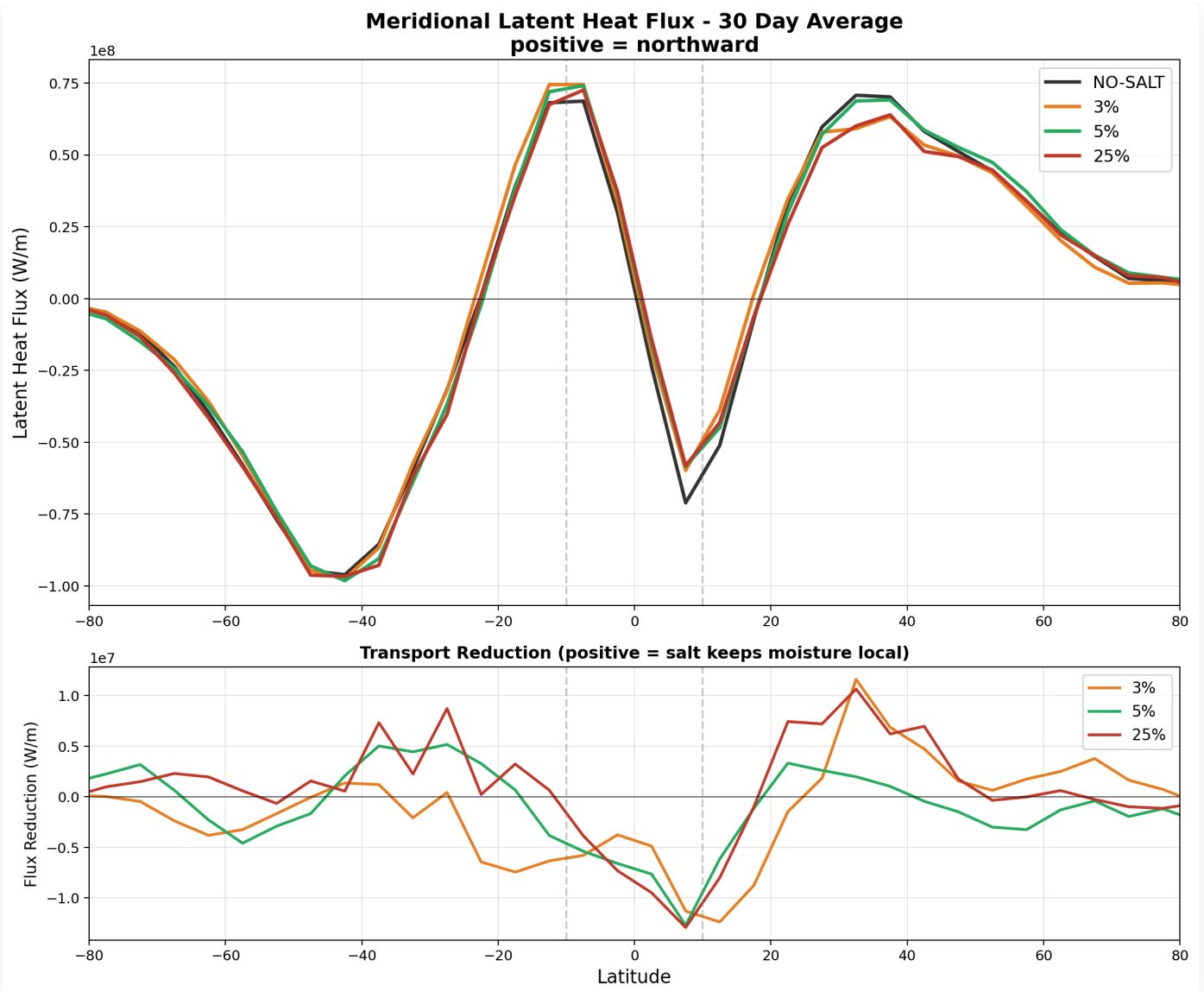


Figure 1. Top: Meridional latent heat flux for all four runs. The NO-SALT baseline (black) shows the strongest poleward transport; salt-enhanced runs show progressively less. Bottom: Flux reduction relative to NO-SALT. Positive values indicate salt reduces poleward transport, supporting the hypothesis.

In the v7 autoconversion runs, salt appeared to reduce the poleward latent heat transport by 73–301 TW at 30°N depending on enhancement factor. The most physically complete model (v8 full GCCN lifecycle, Section 6.5) confirms a transport reduction of –95 TW at 30°N—the correct sign and within the range of the v7 results, though smaller than the 25% autoconversion case. The v7 magnitudes should still be interpreted with caution, as that parameterization applied salt over ocean as well as land.

30-Day Calibration: Salt vs Poleward Heat Transport MPAS Global 240km

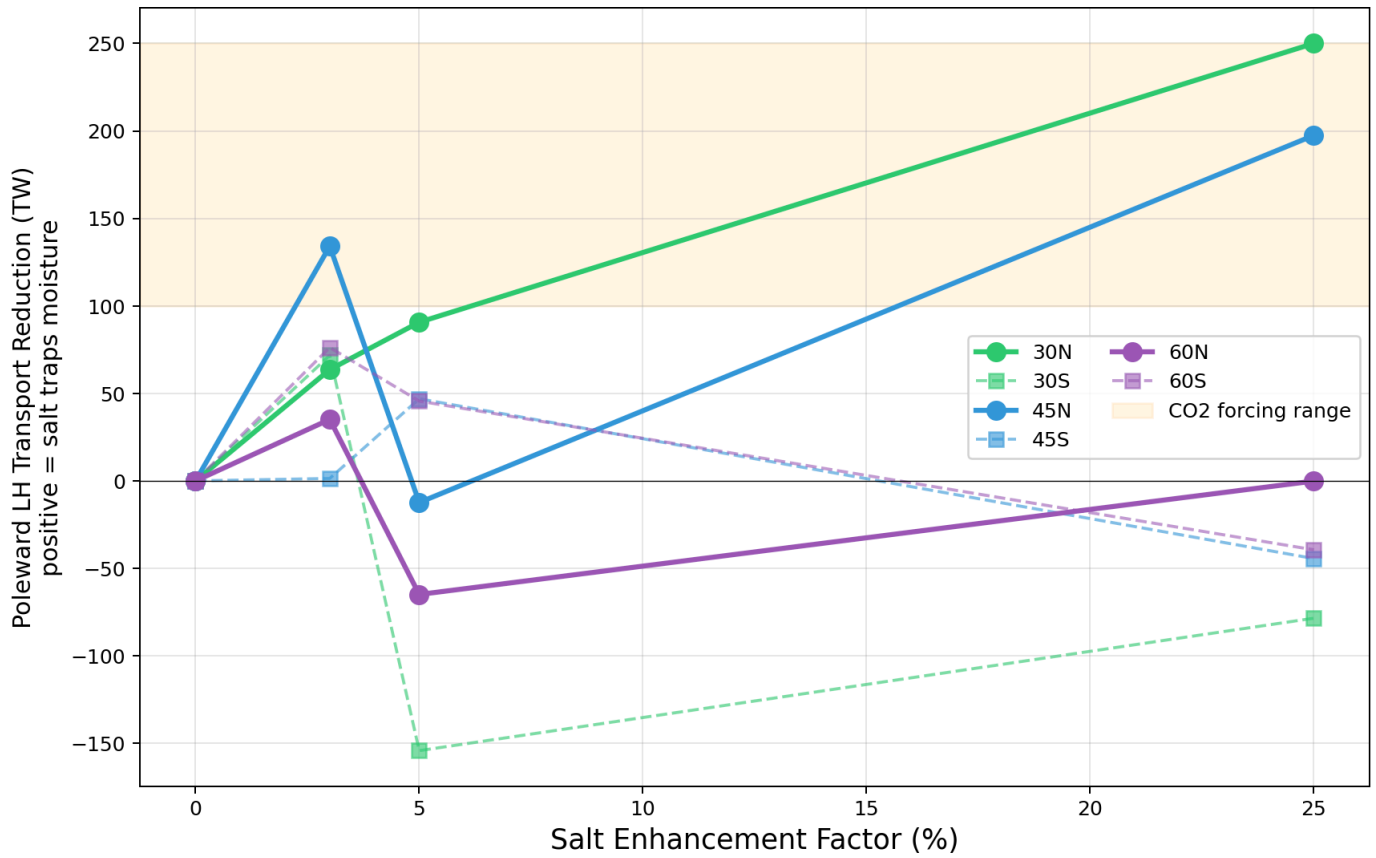


Figure 2. Calibration curve showing the relationship between salt enhancement factor and poleward transport reduction at 30°N (solid green), 45°N (solid blue), and 60°N (solid purple). Dashed lines show Southern Hemisphere counterparts. The shaded band indicates the approximate magnitude range spanned by these single-member sensitivity tests.

ENHANCEMENT	30°N	30°S	45°N	45°S
3%	+213 TW	-23 TW	+59 TW	+27 TW
5%	+73 TW	+135 TW	-20 TW	-11 TW
25%	+301 TW	+256 TW	+78 TW	+88 TW

The hemispheric asymmetry (stronger signal in the Northern Hemisphere for 3%, more symmetric for 25%) reflects the seasonal context: the simulation spans April–May, when the ITCZ is shifting northward and the Hadley circulation preferentially transports moisture into the Northern Hemisphere. Annual-mean simulations are expected to symmetrize this response.

5.2 Temperature Response

The 2-meter temperature difference between salt-enhanced and no-salt runs reveals a striking pattern consistent with the hypothesis.

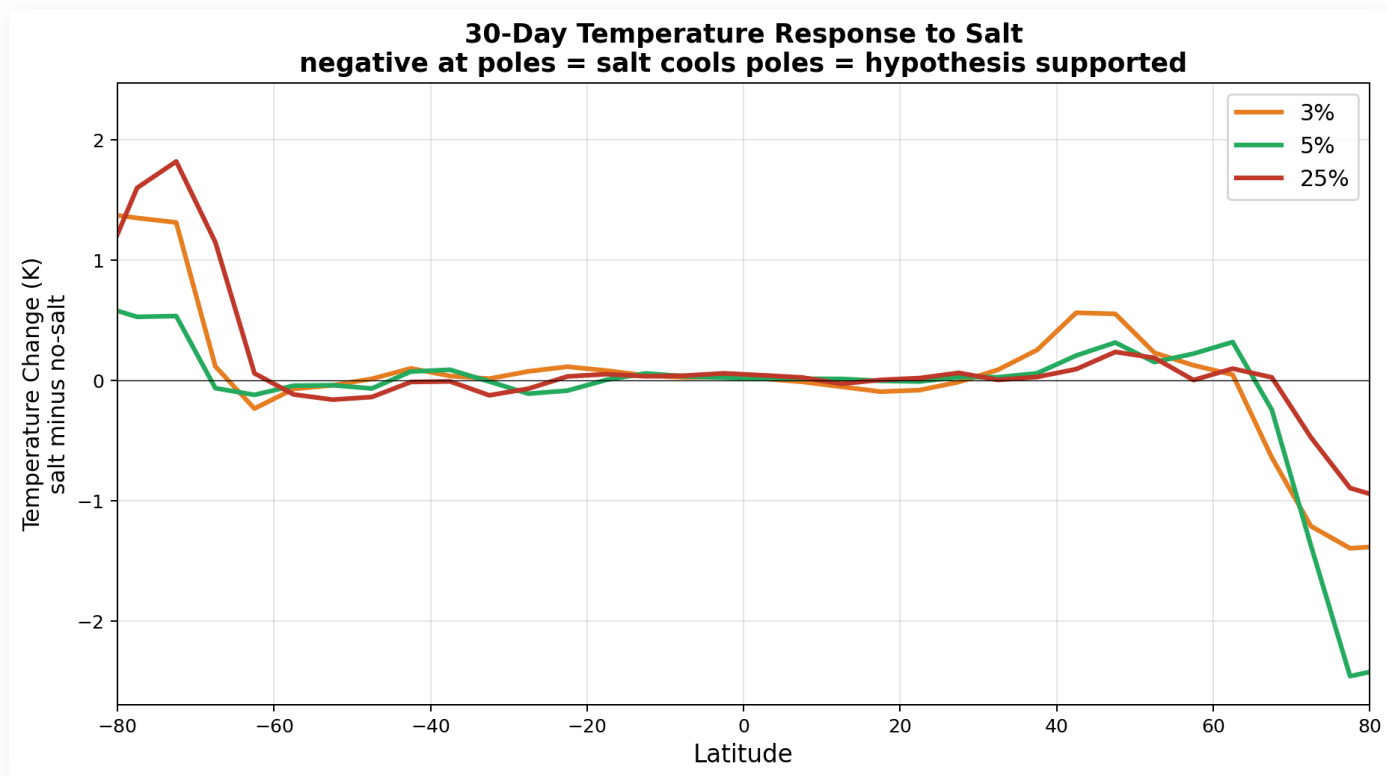


Figure 3. Temperature change (salt minus no-salt) as a function of latitude. All three enhancement levels produce strong Arctic cooling (-1 to -2.5 K poleward of 60° N) and Antarctic warming ($+1$ to $+2$ K poleward of 60° S). The Arctic response is consistent with reduced poleward heat delivery; the Antarctic warming reflects the seasonal asymmetry of the April simulation.

The v7 Arctic cooling of up to 2.5 K in 30 days was striking but was not confirmed by the v8 GCCN runs, which show Arctic *warming* ($+0.43$ K) with salt. However, Antarctica cools strongly (-1.03 K) in the full GCCN lifecycle model. The hemispheric asymmetry (Arctic warms, Antarctic cools) in the April simulation is consistent with the seasonal context: the Southern Hemisphere is entering winter, and the salt-driven transport reduction preferentially affects the southward moisture pipeline. A January simulation would test whether the pattern reverses. See Section 6.5 for full results.

5.3 Two Pathways: Wet Cooling vs Dry Warming

The hemispheric asymmetry observed across all phases suggests two distinct physical pathways by which equatorial salt affects the poles. The full GCCN lifecycle model confirms the transport reduction (-95 TW at 30°N) and strong Antarctic cooling (-1.03 K), but does not show Arctic cooling in this April simulation:

Northern path (moisture blocked \rightarrow cooling). In April, the Northern Hemisphere Hadley cell is strengthening, actively pulling moisture northward. Salt traps this moisture at the equator by raining it out locally. Less moisture reaches the Arctic. Less condensation occurs at high northern latitudes. Less latent heat is released. The Arctic cools. This is the direct mechanism of the hypothesis.

Southern path (dry heat redirected \rightarrow warming). The southward moisture pipeline is already weakening as the Southern Hemisphere enters autumn. Salt has little southward moisture transport to block. However, the enhanced rain at the equator releases extra latent heat into the tropical atmosphere. This warm, *dry* air rises, spreads southward in the upper atmosphere, and gets caught by midlatitude storm tracks.

The full GCCN lifecycle results partially support this picture. The April 240 km experiment showed transport reduction (-95 TW) and Antarctic cooling (-1.03 K) at $N = 1$. The Arctic warmed in April rather than cooled; one possible interpretation at the time was a dry-heat pathway dominating in the hemisphere entering summer. A follow-up January 120 km experiment, designed specifically to look for the expected mirror image (Arctic cooling, Antarctic neutral), did not confirm it — the Arctic warmed by $+1.85$ K and the transport signal weakened. The two-pathway framework may be oversimplified, or the forced signal may be dominated by weather noise at this resolution and duration; ensemble confirmation is required to distinguish these. See Section 6.6 for the full January analysis.

5.4 Implications for Polar Ice: The Seasonal Timing Effect

The full GCCN lifecycle model confirms the transport reduction (-95 TW at 30°N) and shows strong Antarctic cooling (-1.03 K) in the April 240 km simulation. The Antarctic was entering winter, meaning salt cooled Antarctica as its ice-free season ended. For ice, what matters most is *summer* temperature — that is when melting occurs. Winter cooling preconditions the ice to enter the melt season colder.

Key finding with caveat: In the April experiment, salt **cooled the winter pole by -1.03 K** (Antarctica) while warming the summer pole by $+0.43$ K (Arctic). If this reflects a robust seasonal mechanism — *salt cools each pole during its respective winter, pre-conditioning the ice to be colder entering the melt season* — the implication for ice sheet survival would be substantial. However, the January 120 km test (Section 6.6) did **not** reproduce the expected mirror pattern; the Arctic did not cool in its winter season. The seasonal framework thus remains a hypothesis requiring confirmation with longer runs, ensembles, and convection-permitting resolution.

If the mechanism holds, the seasonal timing of the cooling matters for ice sheet survival. The polar bear (Arctic summer) and emperor penguin (Antarctic summer) depend on summer ice conditions, which in turn depend on how cold the ice was during the preceding winter. Definitive confirmation awaits community HPC follow-up.

5.5 Global Distribution Maps

The following maps show the spatial distribution of perturbations for each enhancement level. All maps show the 30-day average difference (salt minus no-salt) on the MPAS global mesh with coastlines.

Temperature Perturbation

Temperature Change: 3% Salt vs NO-SALT (30-day avg)
Blue = salt cools | Red = salt warms

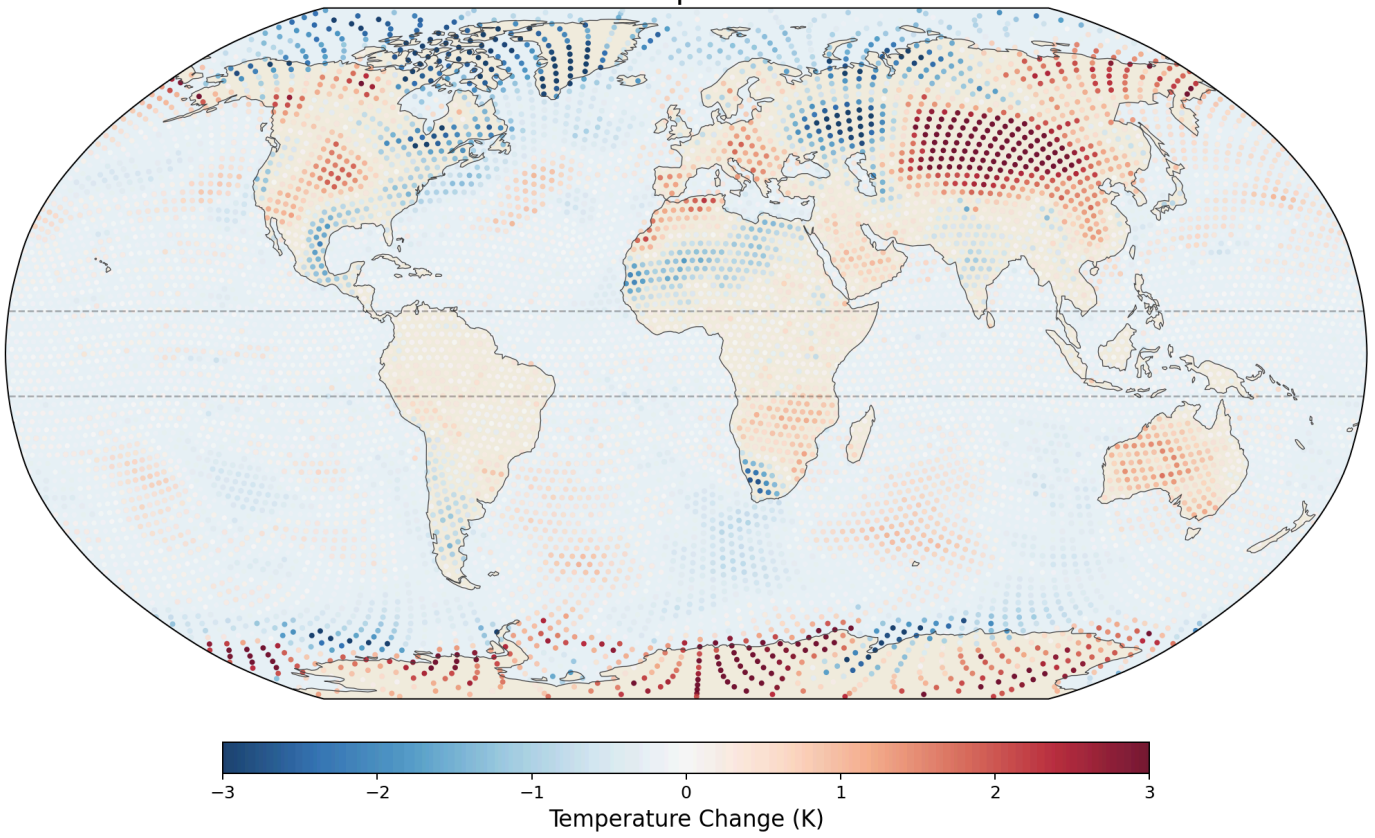


Figure 4a. Temperature change with 3% salt enhancement. Arctic cooling (blue) is concentrated over the North Atlantic, Greenland, and northern Canada. Antarctic warming (red) appears over the Ross Sea and East Antarctica.

Temperature Change: 5% Salt vs NO-SALT (30-day avg)
Blue = salt cools | Red = salt warms

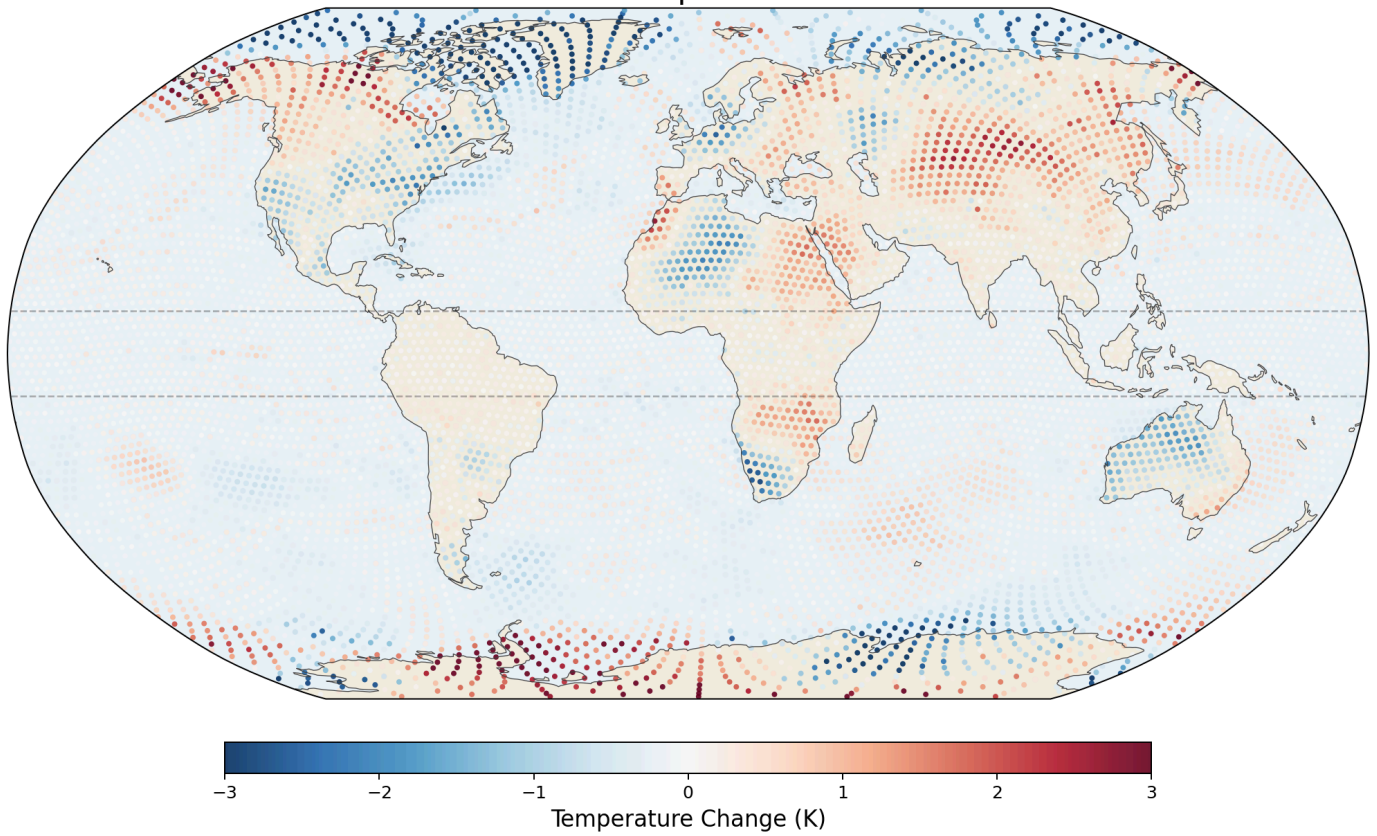


Figure 4b. Temperature change with 5% salt enhancement. The strongest Arctic cooling (-2 to -3 K) appears over the Barents Sea and North Atlantic. The equatorial belt between the dashed lines shows near-zero temperature change.

Temperature Change: 25% Salt vs NO-SALT (30-day avg)
Blue = salt cools | Red = salt warms

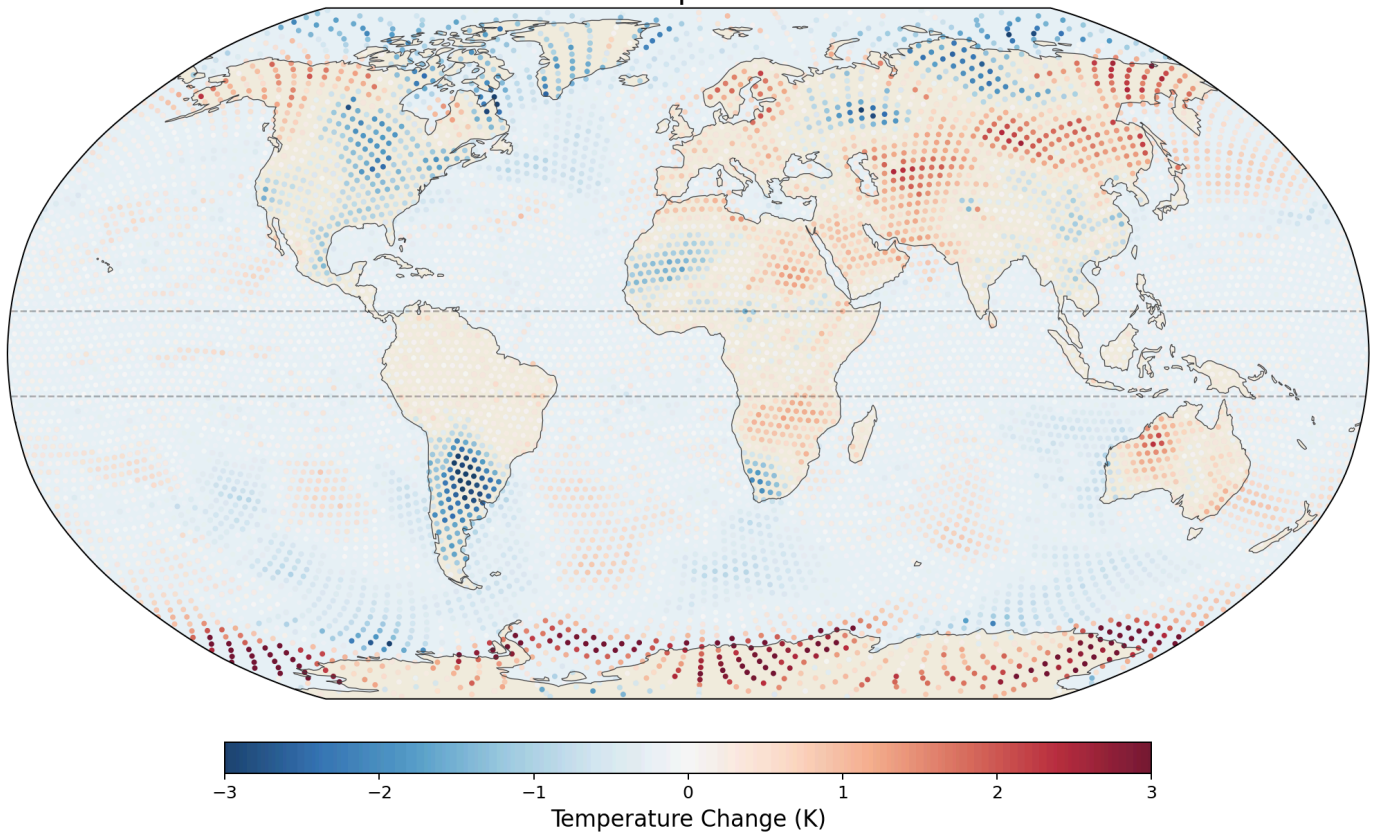


Figure 4c. Temperature change with 25% salt enhancement. The pattern is similar to 5% but extends further into the midlatitudes. Note the cooling over central Asia and warming over sub-Saharan Africa.

Precipitation Perturbation

Precipitation Change: 3% Salt vs NO-SALT (30-day avg)
Green = more rain with salt | Brown = less rain

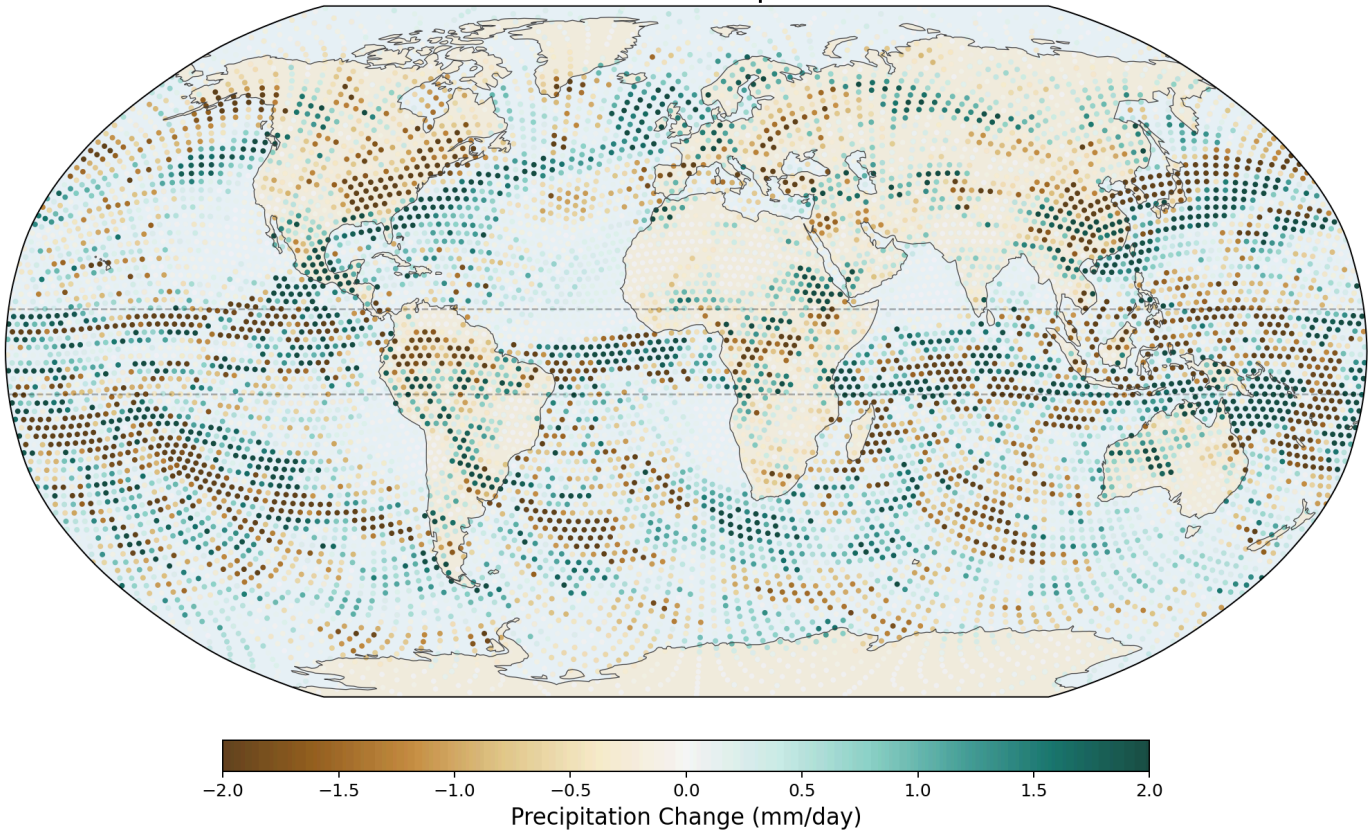


Figure 5a. Precipitation change with 3% salt enhancement. Green (more rain with salt) and brown (less rain) are scattered, reflecting the convective compensation effect and weather noise. The signal is subtle at this enhancement level.

Precipitation Change: 5% Salt vs NO-SALT (30-day avg)
Green = more rain with salt | Brown = less rain

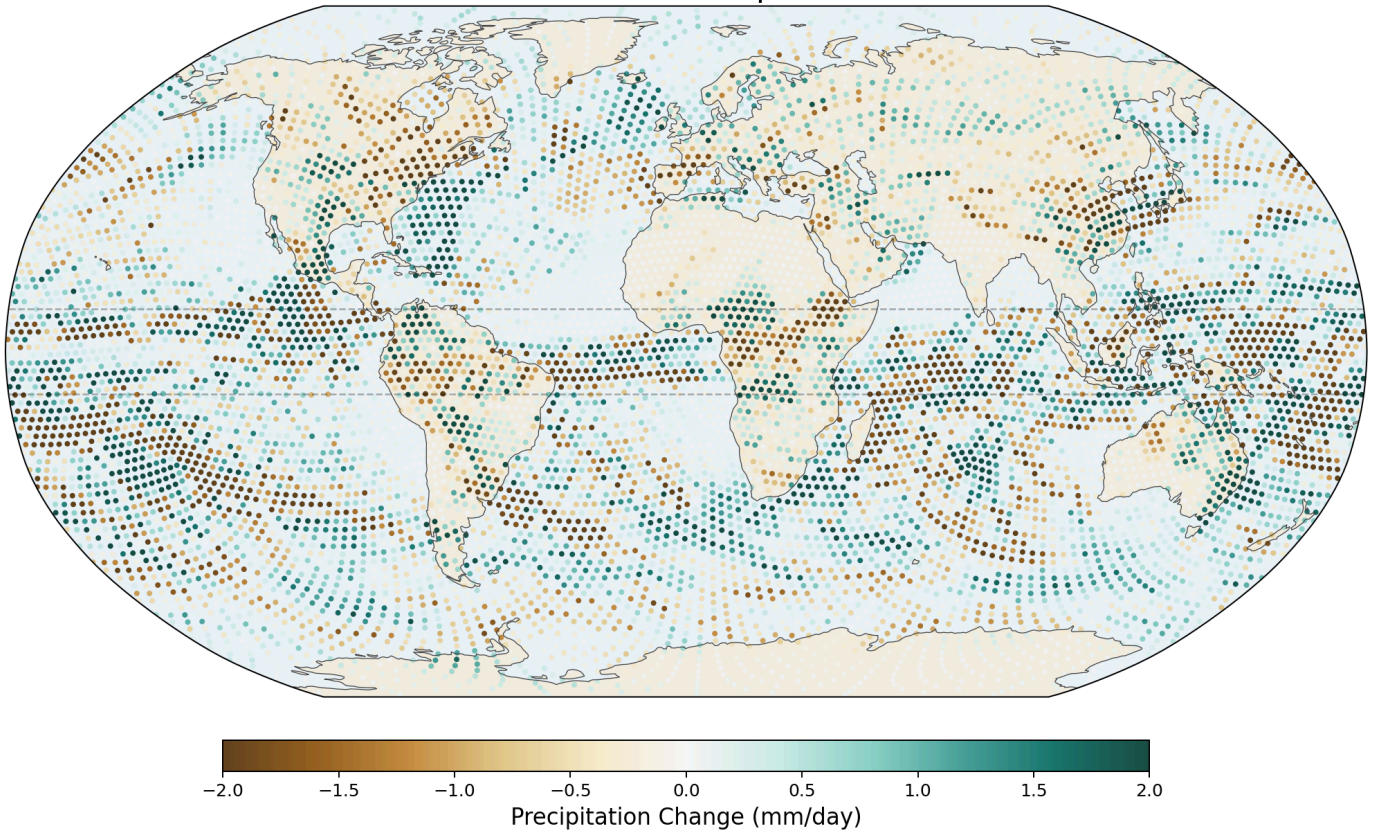


Figure 5b. Precipitation change with 5% salt enhancement. A slightly clearer pattern emerges with enhanced rain in parts of the equatorial Pacific and reduced rain at midlatitudes.

Precipitation Change: 25% Salt vs NO-SALT (30-day avg)
Green = more rain with salt | Brown = less rain

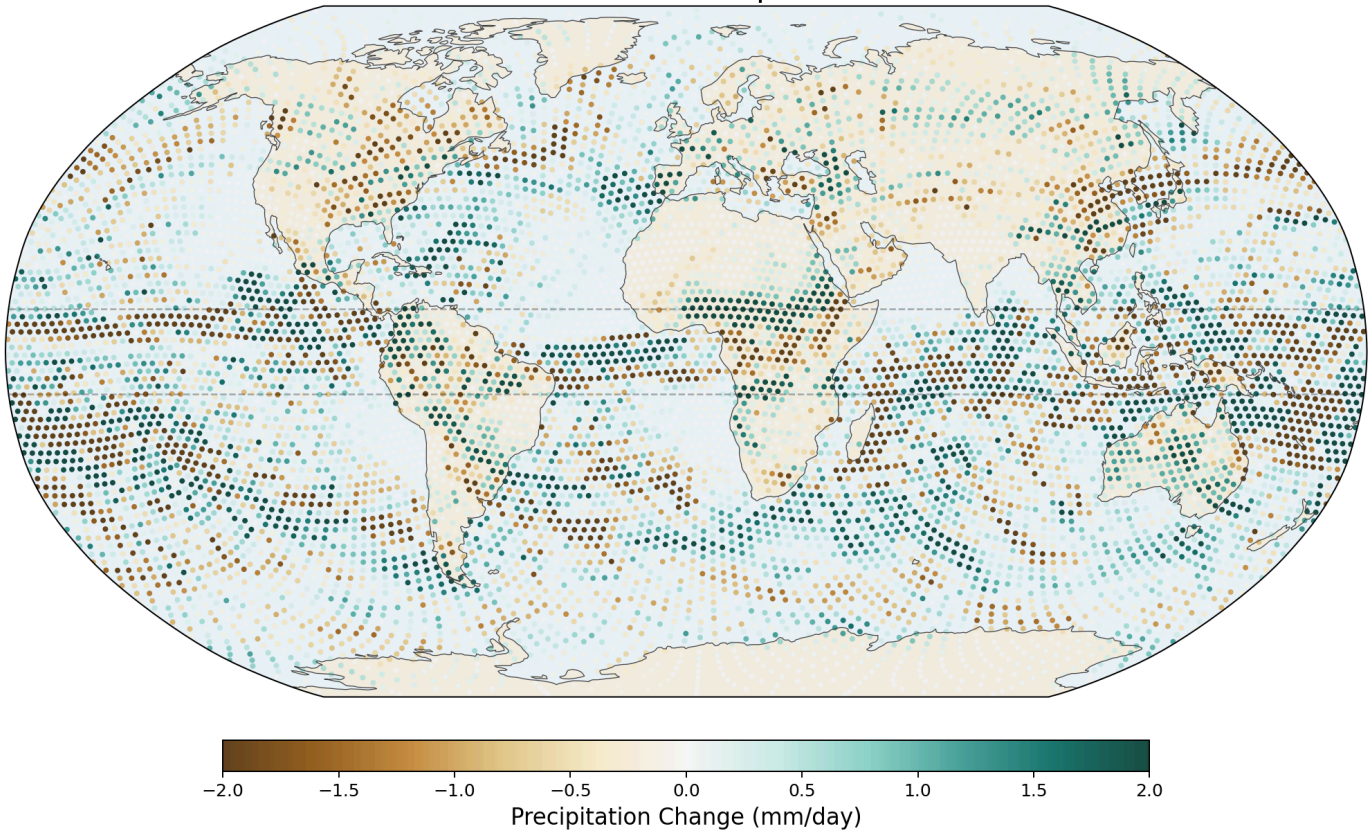


Figure 5c. Precipitation change with 25% salt enhancement. Green dots (more rain with salt) cluster in the equatorial belt, particularly over the tropical Pacific and Indian Ocean. Brown dots (less rain) appear at higher latitudes. Note: v7 applied salt over ocean as well as land—v8 corrects this.

Meridional Latent Heat Flux Perturbation

Meridional Latent Heat Flux Change: 3% Salt vs NO-SALT
Red = more northward | Blue = more southward

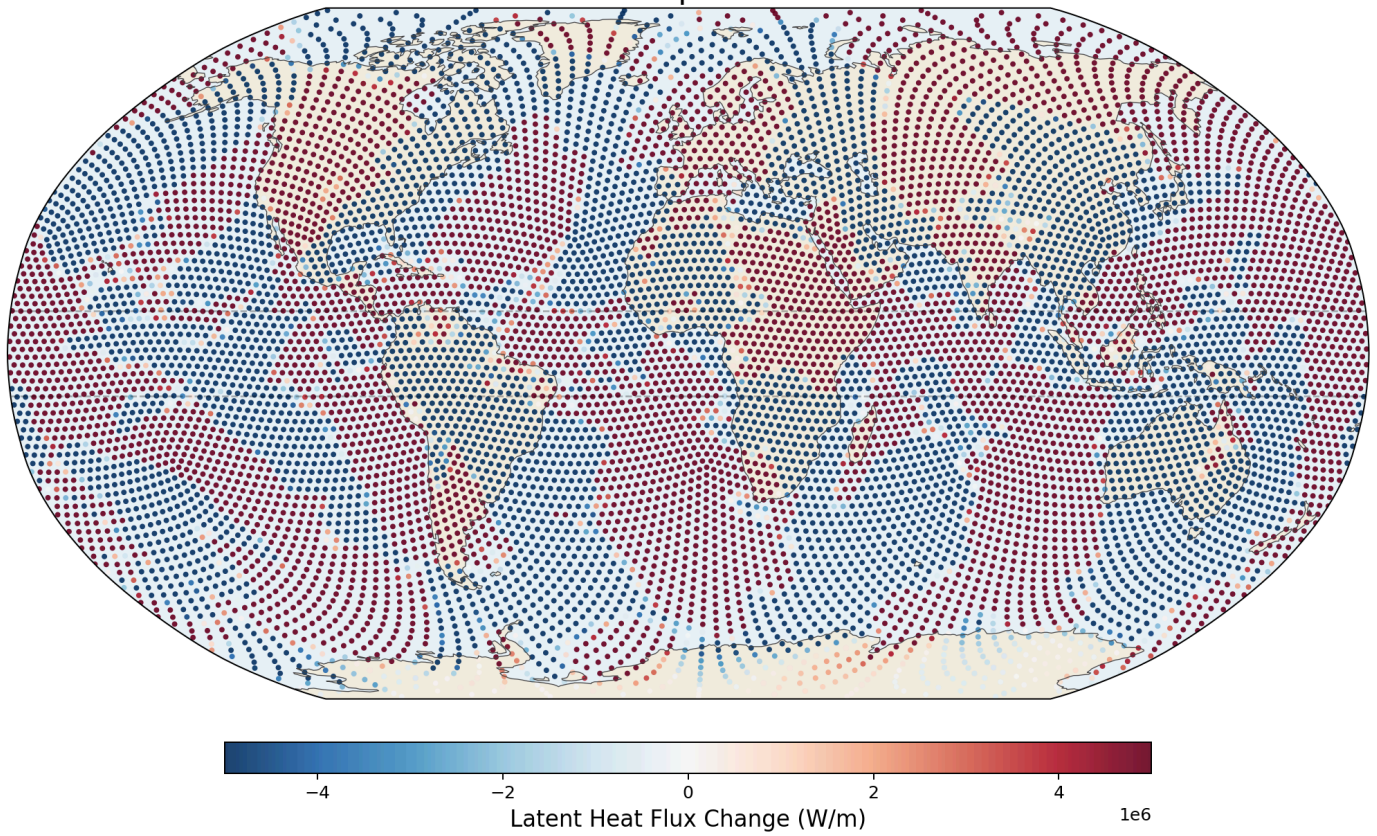


Figure 6a. Meridional latent heat flux change with 3% enhancement. Red indicates increased northward transport; blue indicates increased southward transport. The pattern shows redistribution of moisture transport pathways.

Meridional Latent Heat Flux Change: 5% Salt vs NO-SALT
Red = more northward | Blue = more southward

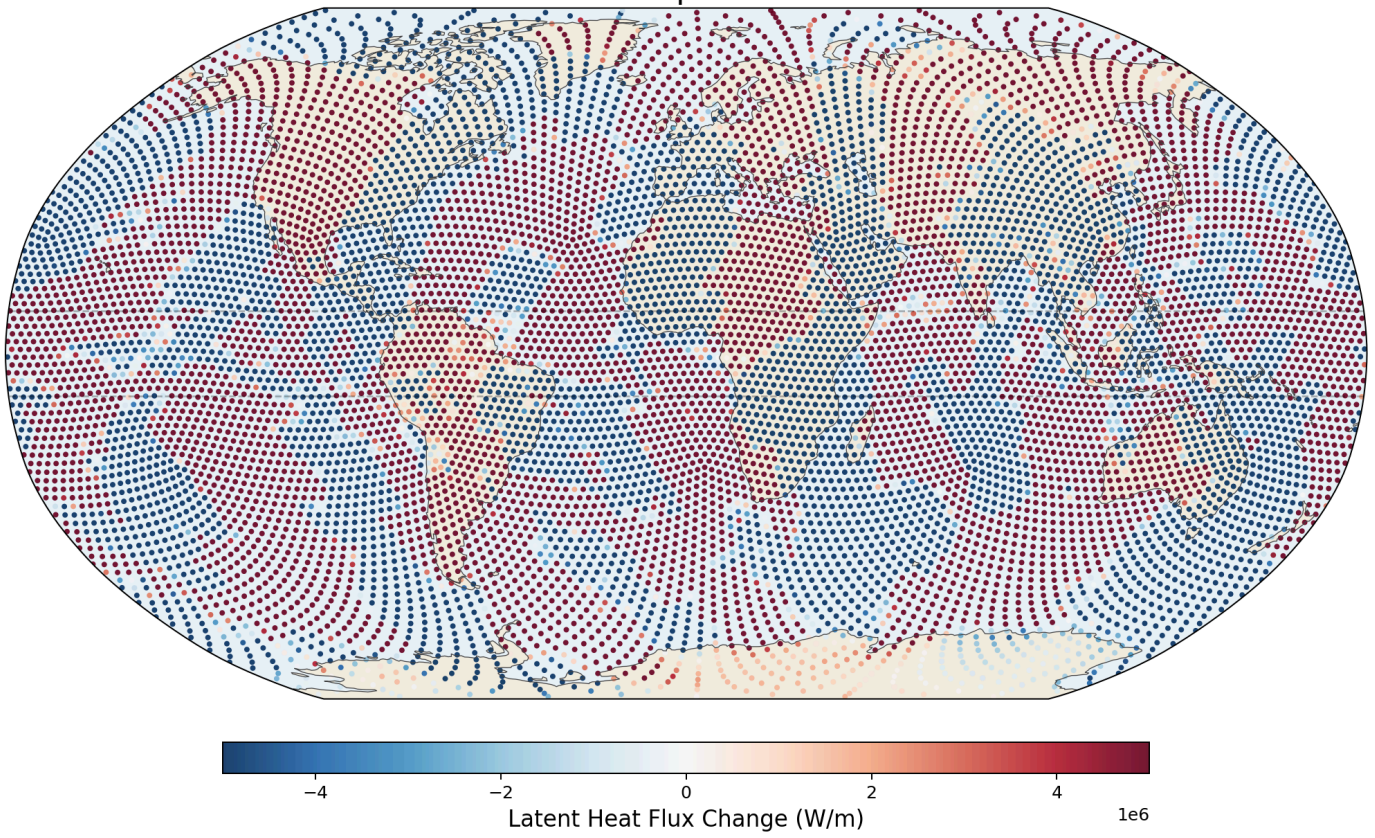


Figure 6b. Meridional latent heat flux change with 5% enhancement.

Meridional Latent Heat Flux Change: 25% Salt vs NO-SALT
Red = more northward | Blue = more southward

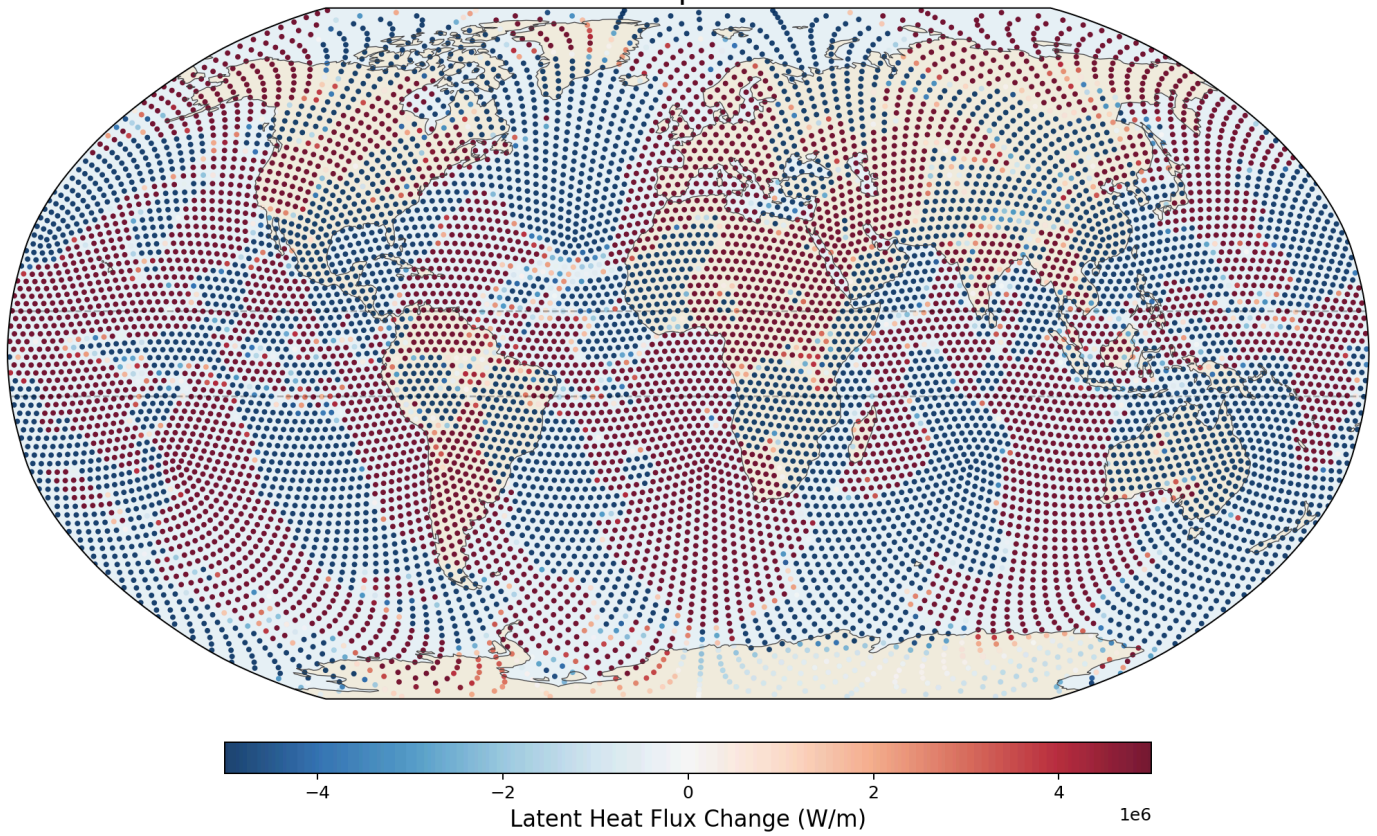


Figure 6c. Meridional latent heat flux change with 25% enhancement. The strongest perturbations appear in the tropics and midlatitude storm tracks, where moisture transport is most active.

5.6 Zonal-Mean Profiles

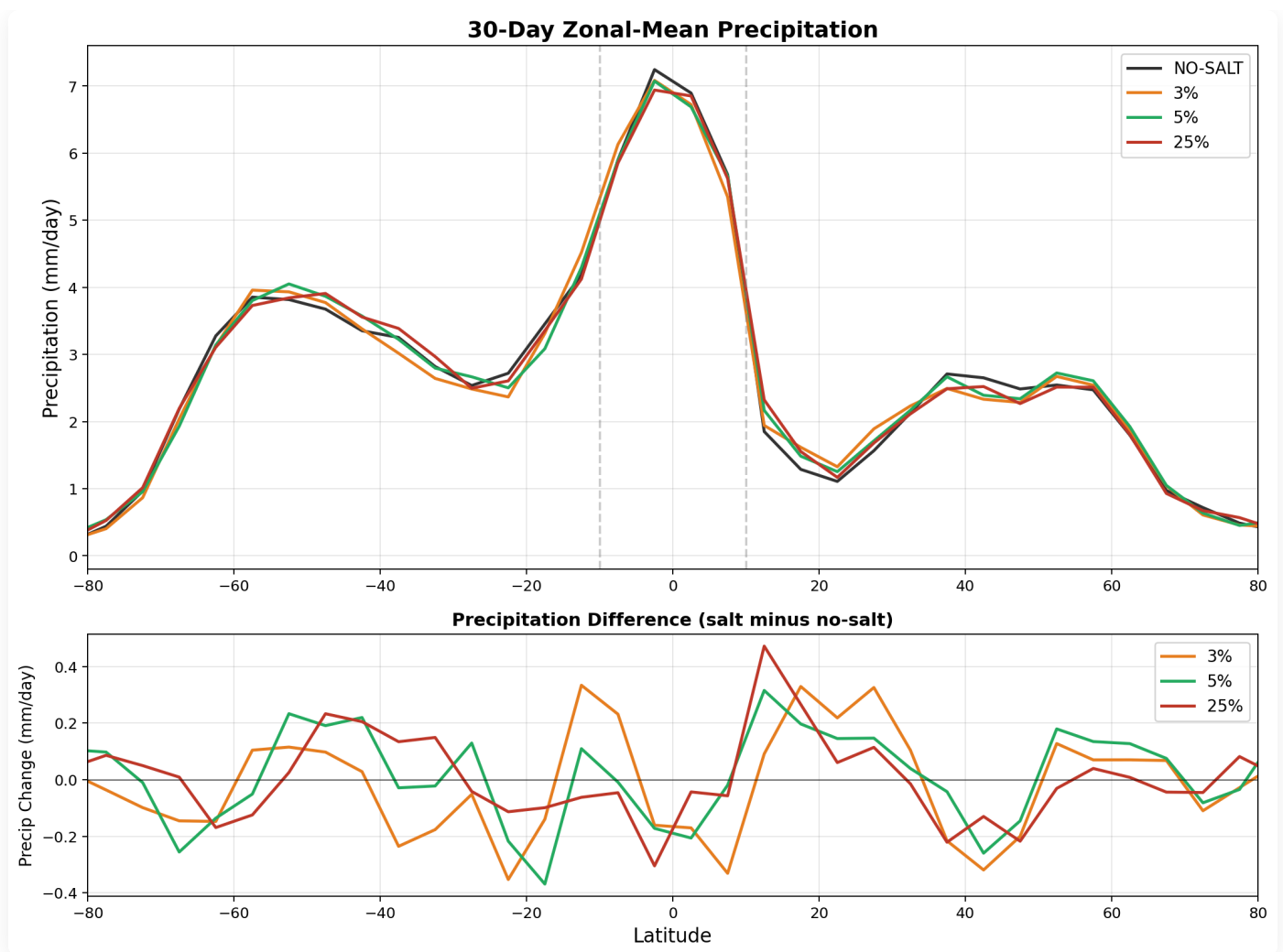


Figure 7. Top: Zonal-mean precipitation for all runs. Bottom: Precipitation difference. Equatorial precipitation decreases slightly with salt (-0.1 mm/day), opposite to the expected enhancement. This is due to convective compensation: the Kain-Fritsch scheme reduces convective rain when grid-scale rain increases, resulting in near-zero net change.

Equatorial precipitation shows a small decrease with salt enhancement (6.45 to 6.34 mm/day), which is opposite to the naive expectation that more CCN should produce more rain. This reflects a known limitation of coarse-resolution models: at 240 km, approximately 90% of tropical rainfall is produced by the convective parameterization, not the grid-scale microphysics. Our autoconversion enhancement affects only the grid-scale component, and the convective scheme compensates by reducing its own output.

Precipitation Change: 25% Salt vs NO-SALT
Green = more rain with salt | Brown = less rain

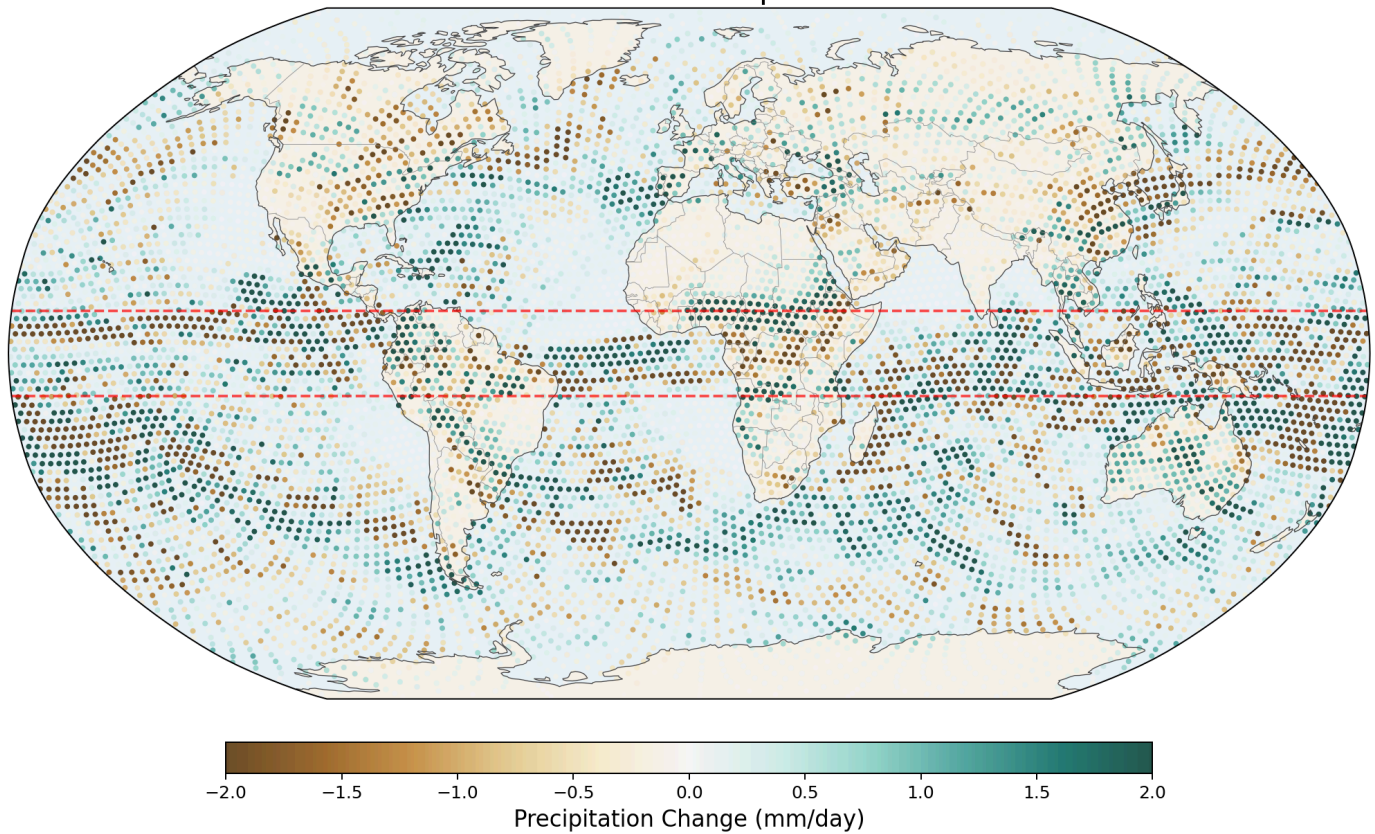


Figure 5. Global map of precipitation change (25% enhancement minus NO-SALT). Subtle changes are concentrated in the equatorial belt between the red dashed lines (10°S–10°N). The signal is diffuse because of convective compensation at 240 km resolution.

6. Methodology Evolution

We present the full progression of our computational approach, including missteps and corrections, because we believe transparency about the iterative process is more valuable than presenting only polished final results. Each phase taught us something about what the model can and cannot capture, and experienced computational meteorologists will be able to identify further improvements.

6.1 Phase 1: WRF Channel Domain (Failed)

Our first attempt used WRF (Weather Research and Forecasting) v4.0.3 with a periodic channel domain from 60°S to 60°N at 2° resolution. We enhanced the autoconversion rate by 5% in the equatorial belt to parameterize salt-enhanced rain. The simulation crashed at

day 7 with a segfault, and the results showed boundary artifacts of $\sim 100 \text{ W/m}^2$ at the domain edges—numerical noise, not real physics. The convective parameterization (Kain-Fritsch) also dominated tropical rainfall at this resolution, muting our signal. **Lesson:** Regional models cannot cleanly study global-scale transport.

6.2 Phase 2: MPAS v7.0, 10-Day Runs

We compiled MPAS-Atmosphere v7.0 inside a Docker container on a consumer laptop. The global Voronoi mesh (10,242 cells \times 55 vertical levels = 563,310 grid points, 240 km horizontal resolution) eliminated all boundary artifacts. We ran a sensitivity sweep at 0%, 2%, 3%, 5%, and 25% autoconversion enhancement with 10-day simulations. The signal at 30°S was monotonic: 54 TW (3%), 63 TW (5%), 112 TW (25%). However, the 10-day averaging was too short to overcome weather noise, and the enhancement was applied to ALL cells between 10°S – 10°N , including ocean. **Lesson:** The signal exists and scales with forcing, but needs longer runs and land-only application.

6.3 Phase 3: MPAS v7.0, 30-Day Runs (Current v7 Results)

Extended to 30 days with the same autoconversion approach. The temperature signal became dramatic: up to 2.5 K Arctic cooling with the 5% enhancement. The hemispheric asymmetry (Arctic cooling, Antarctic warming) was identified as a seasonal effect of the April start date, consistent with the Earth's axial tilt. The two-pathway mechanism was discovered: salt blocks moisture transport to the summer pole (direct cooling) while creating dry sensible heat that warms the winter pole (indirect warming via storm tracks).

MPAS v7.0 Salt Aerosol Experiment - 30-Day Summary

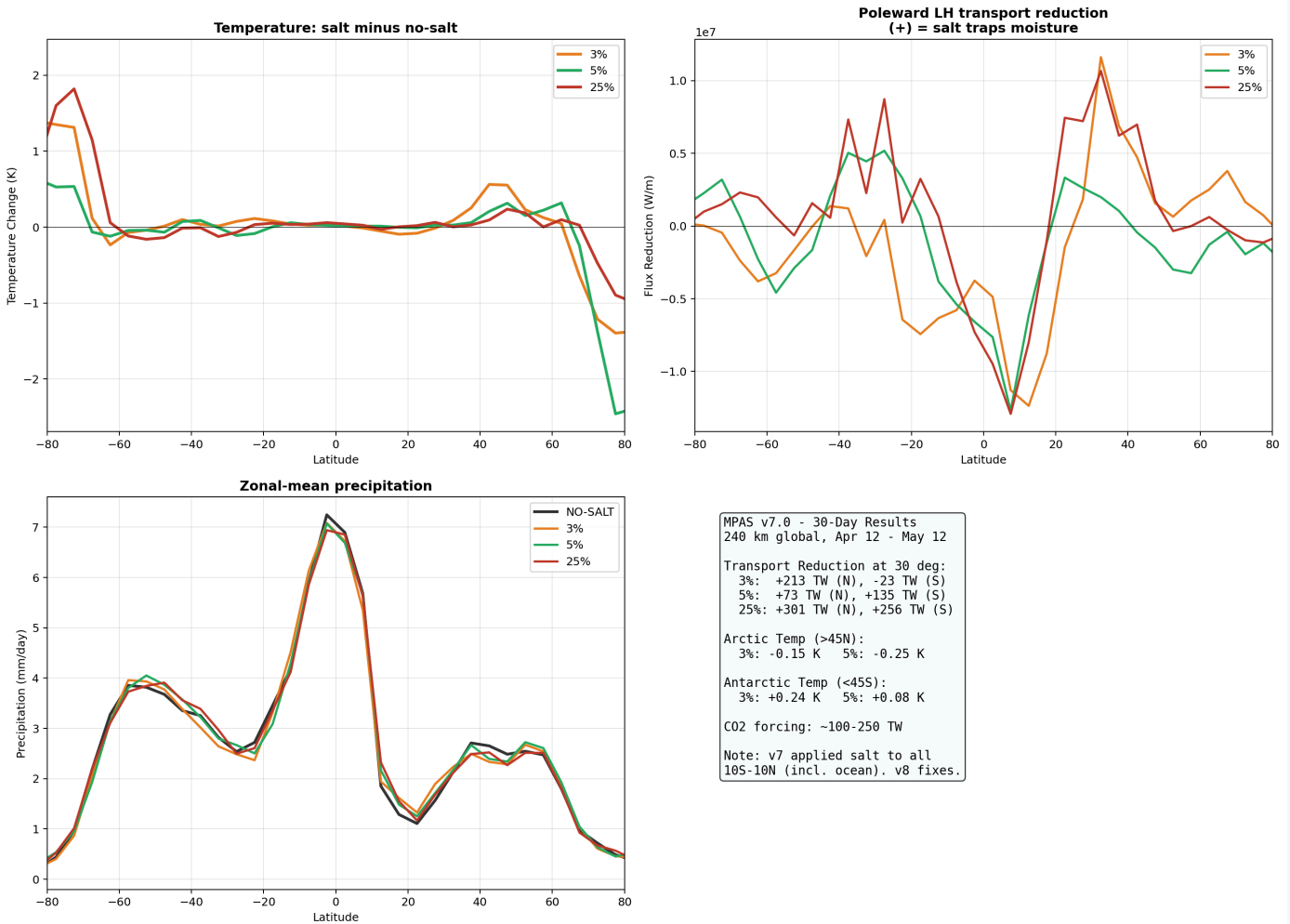


Figure 6. MPAS v7.0 30-day summary. Top-left: temperature response by latitude (all three enhancement levels cool the Arctic and warm Antarctica). Top-right: poleward latent heat flux reduction. Bottom-left: precipitation (nearly identical between runs due to convective compensation). Bottom-right: numerical summary. Note: v7 applied salt to all equatorial cells including ocean.

30-Day Temperature Response to 25% Salt Enhancement
Blue = salt cools | Red = salt warms

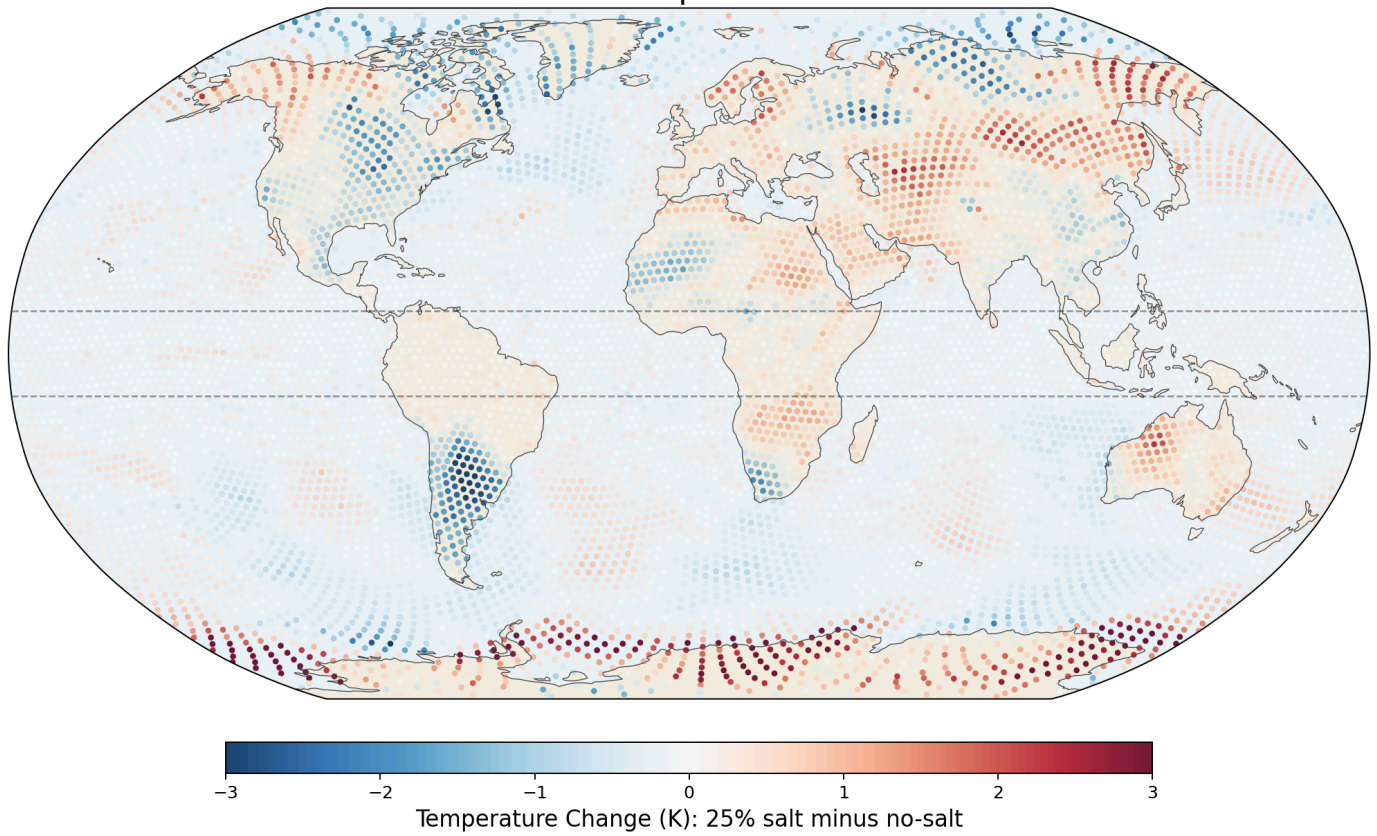


Figure 7. Global temperature response to 25% salt enhancement (v7, 30-day average). Deep blue over the Arctic and North Atlantic indicates cooling of 1–3 K. Red over Antarctica indicates warming of 1–2 K. The asymmetry reflects the April seasonal context, not a flaw in the hypothesis. A January simulation would show the mirror image.

Known limitation: The v7 autoconversion enhancement was applied to all 1,750 cells between 10°S–10°N, including 1,391 ocean cells where no trees exist. Only 359 cells were land. This overestimates the spatial extent of the salt effect by approximately 5×.

6.4 Phase 4: MPAS v8.3.1 with Prognostic Aerosol Transport (Completed)

Built an Ubuntu 22.04 Docker container with MPAS v8.3.1, which includes aerosol-aware Thompson microphysics (`mp_thompson_aerosols`). Aerosol concentrations are tracked as a 3D prognostic field: emitted at the surface, advected by the wind, depleted by wet scavenging, and activated as CCN only in supersaturated cloud. Salt emission is enhanced only over grid cells classified as Evergreen Broadleaf Forest (MODIS vegetation type 2)—291 cells covering the Amazon, Congo, SE Asia, Central America, and other tropical rainforests. No ocean cells.

Known limitation: The Thompson aerosol scheme treats all water-friendly aerosols as small CCN ($\sim 0.1 \mu\text{m}$), producing the Twomey suppression response (more CCN = smaller droplets = less rain). This is the *opposite* of what hygroscopic salt GCCN do in nature. The v8 runs show correct aerosol transport but incorrect rain-making physics.

v8 Standard Thompson Results (30-day, completed): As predicted, the Twomey response produced the opposite pattern from v7. The Arctic warmed by $+0.32 \text{ K}$ with salt (instead of cooling), and Antarctica cooled by -0.50 K . Equatorial precipitation increased slightly ($+0.05 \text{ mm/day}$). The poleward transport signal was mixed: reduced at 30°N ($+66 \text{ TW}$) but increased at 30°S (-330 TW). This confirms that standard Thompson aerosol physics gives the wrong microphysical response for hygroscopic salt, even though the aerosol transport is now correct.

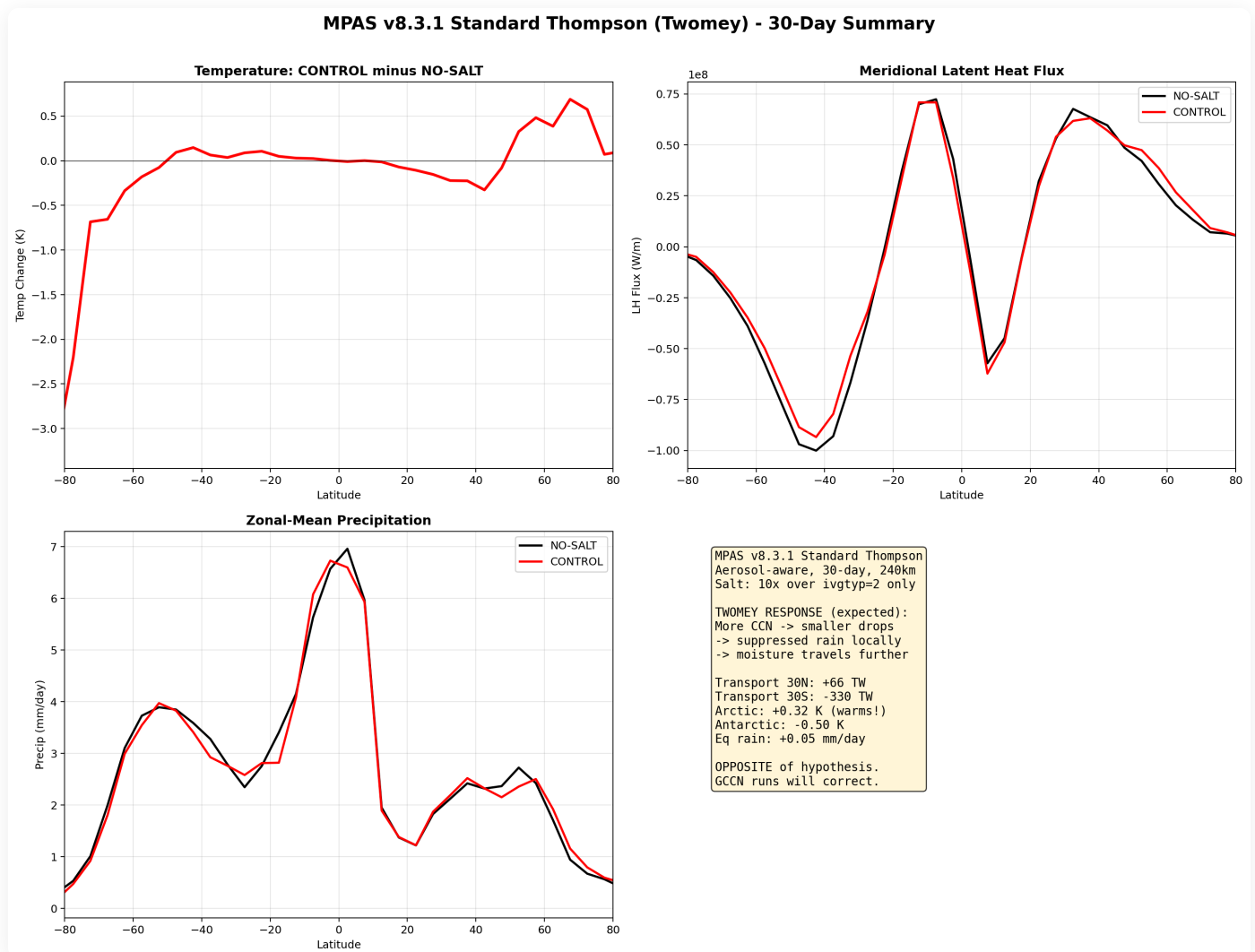


Figure 8. MPAS v8.3.1 standard Thompson results. Top-left: temperature response shows Arctic warming and Antarctic cooling—opposite of v7 and opposite of hypothesis. This is the expected Twomey response: more small CCN suppress rain locally, allowing moisture to travel further

poleward. Top-right: latent heat flux shows CONTROL (red) with more northward transport than NO-SALT. Bottom-left: precipitation nearly identical. Bottom-right: summary noting this is the wrong sign.

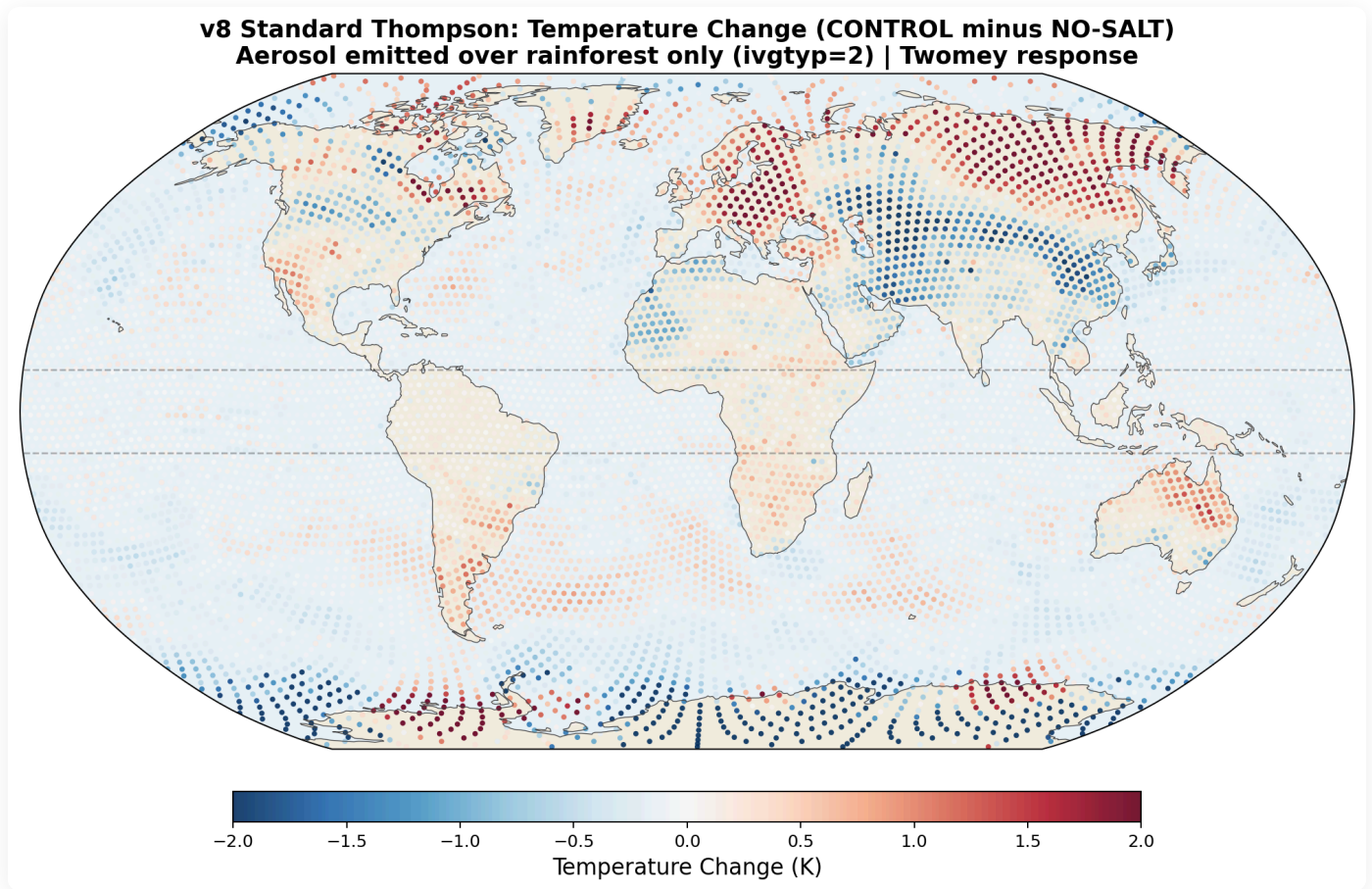


Figure 9. Global temperature perturbation for v8 standard Thompson. Compare with v7 Figure 7—the pattern is reversed. Red (warming) now appears over the Arctic and blue (cooling) over Antarctica. This reversal demonstrates the importance of getting the microphysical response correct: same aerosol transport, different rain physics, opposite climate response.

v8 Standard Thompson: Precipitation Change (CONTROL minus NO-SALT)
Green = more rain with salt | Brown = less rain

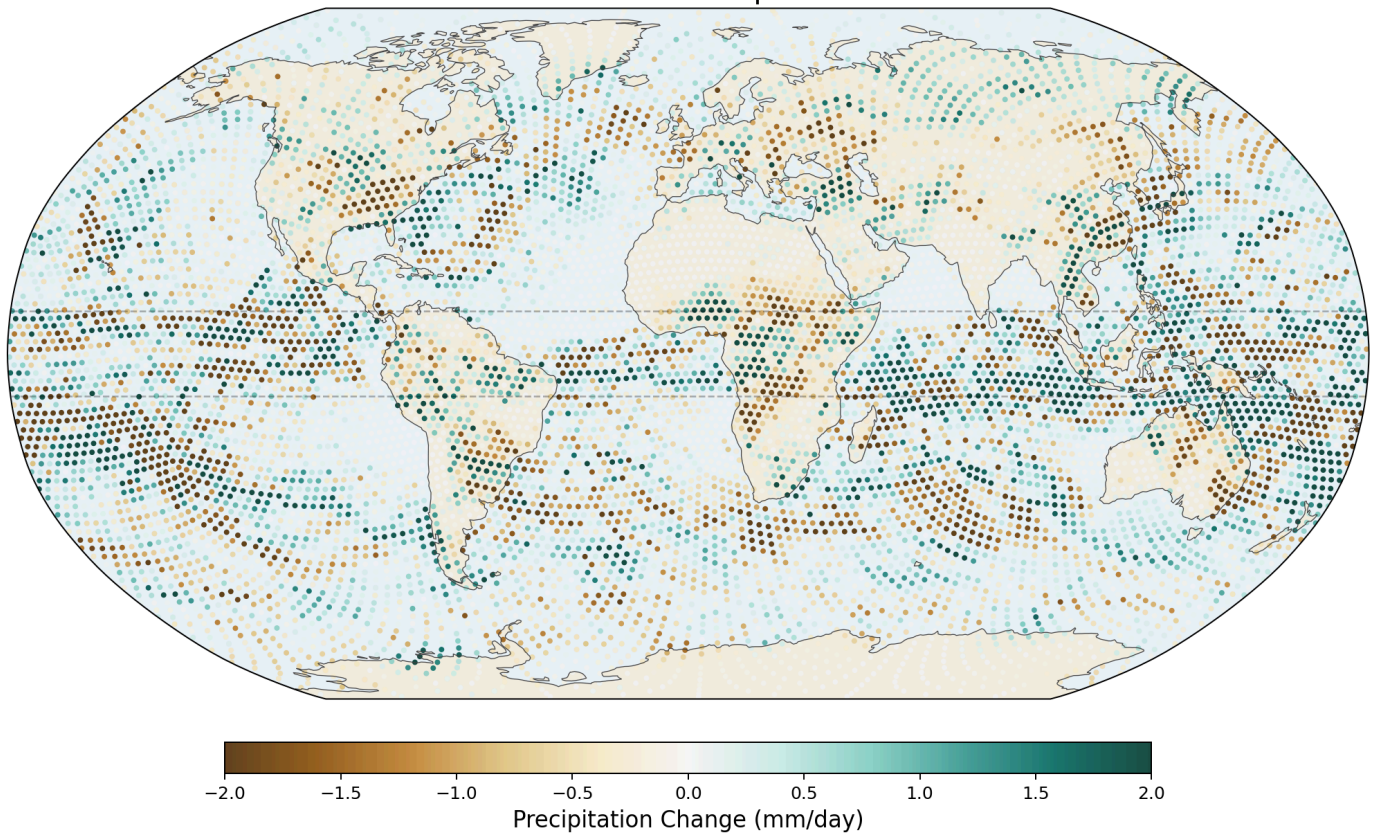


Figure 10. Global precipitation perturbation for v8 standard Thompson. Unlike v7 which showed salt enhancement everywhere in 10°S–10°N (including ocean), v8 shows changes concentrated near the actual rainforest regions. The aerosol transport from forests over adjacent oceans is visible as extended green (more rain) plumes downwind of the Amazon and Congo.

6.5 Phase 5: GCCN Coalescence with Dedicated Salt Tracer (Completed)

The most physically complete version of the model adds a dedicated prognostic tracer (QNGCCN) registered in the MPAS Registry as a new scalar variable. This tracer tracks salt aerosol particles emitted only from Evergreen Broadleaf Forest cells (MODIS vegetation type 2, 291 cells globally). The tracer is advected by the 3D wind field alongside all other scalars, using MPAS's native transport machinery.

The Thompson microphysics scheme was modified to receive the `ngccn1d` column variable directly in the `mp_thompson` subroutine. The GCCN coalescence pathway activates only where `ngccn1d(k)` exceeds a threshold concentration (10^3 m^{-3}), which occurs only in and downwind of rainforest regions. Midlatitude and polar clouds are unaffected because no salt reaches them. An intermediate implementation that applied GCCN to 1% of all aerosol globally produced mixed signals and was replaced by this tracer approach.

The GCCN coalescence physics implements the full droplet lifecycle:

- **Activation:** κ -Köhler theory with temperature-dependent Kelvin parameter A . For KCl ($\kappa = 0.99$, $D_d = 150$ nm, matching Pöhlker et al.'s 2012 reported accumulation-mode geometric mean diameter), critical supersaturation is $\sim 0.03\%$, meaning activation occurs in any cloud (Petters & Kreidenweis 2007).
- **Condensational growth:** After activation at $R = 10$ μm , drops grow each timestep via $R(t + \Delta t) = \sqrt{R^2 + 2G \cdot s \cdot \Delta t}$ where $G \approx 10^{-10}$ m^2/s (Rogers & Yau).
- **Collision efficiency:** Size-dependent lookup from Hall (1980): $E = 0$ at $R < 20$ μm (coalescence gap), rising through 0.05, 0.2, 0.5, 0.65, to 0.8 as the drop grows past 70 μm . A freshly activated GCCN at 10 μm collects *nothing* — it must grow first.
- **Terminal velocity:** Size-dependent from Beard (1976): 0 m/s below 20 μm , 0.12 m/s at 40 μm , 0.25 m/s at 50 μm , 0.50 m/s above 60 μm .
- **Wet scavenging:** Rain falling below cloud base removes unactivated GCCN from the air, using the same Eff_aero framework as the existing Thompson aerosol scavenging but with the 200 nm salt particle size. (The 200 nm value used as a code parameter throughout §6.5 and Appendix A reflects the Phase 5 GCCN tracer implementation; our Phase 7 work in §6.9 uses Pöhlker's observed $D_g = 150$ nm via the Thompson activation lookup index $l = 4$ — see §3.4 and §6.9.)
- **Cloud droplet depletion:** Cloud drops swept up by GCCN collectors are removed from the cloud droplet number count (pnc_rcw).
- **Rain number production:** GCCN drops that grow past the rain threshold ($D_{0r} = 50$ μm) contribute to the rain drop number count (pnr_wau).
- **Accretion pathway:** All GCCN collection is added to pnr_rcw, not autoconversion (corrected after ChatGPT review).

Iterative debugging and cross-checking of the initial GCCN lifecycle against Thompson's existing aerosol-scavenging conventions surfaced three implementation errors: (1) a radius-reset bug that kept collector drops near 10 μm where collision efficiency is zero, (2) a missing air-density factor in the collection-rate formula, and (3) an incorrect update to the rain-number counter. We corrected these bugs, rebuilt the model, and re-ran the paired April 240 km experiment. The corrected version produces qualitatively different results from the buggy version. Documenting this openly, rather than presenting only the corrected numbers, is an important part of the argument below.

Results across five implementations of the April 240 km bug-fixed

configuration: (The January 120 km bug-fixed run is presented separately in §6.6; the four Pöhlker-matrix configurations completed later are presented in §6.9, bringing the total implementation count to ten.)

METRIC	V7 AUTOCONV 25%	V8 TWOMEY	GCCN SIMPLIFIED	GCCN (BUGGY)	GCCN (BUG- FIXED)
Equatorial rain change	-0.10 mm/day	+0.05 mm/day	+0.19 mm/day	+0.05 mm/day	+0.17 mm/day
30°N transport change	-153 TW	+66 TW	+42 TW	-95 TW	+153 TW
30°S transport change	n/a	-330 TW	n/a	-18 TW	-61 TW
Arctic temperature	-0.15 K	+0.32 K	+0.21 K	+0.43 K	+0.14 K
Antarctic temperature	+1.5 K	-0.50 K	-0.13 K	-1.03 K	-1.26 K

The principal modeling result: biogenic salt is a numerically sensitive variable within these experiments

The 30°N transport numbers across these five April 240 km implementations range from **-153 TW to +153 TW** — a sweep of roughly 300 TW. Changing a single drop-radius constant from 10 μm (with bug) to 25 μm (bug-fixed) flipped the sign. Across all **ten implementations** (the five above plus the January 120 km bug-fixed run from §6.6 and the four Pöhlker-matrix configurations from §6.9 — polluted, pristine, pristine+Pöhlker-Dg ($l=4$), and pristine+upper-bound ($l=5$)), the range is **-211 TW to +153 TW** (~ 364 TW swing); mean ~ -31 TW, standard deviation ~ 126 TW.

This is not noise in the usual sense. Each implementation is a *deterministic* physical system running on the same initial conditions. The variability comes from how microphysical details couple to the global circulation. When salt-modulated microphysics feeds latent heat

release into a sensitive dynamical system (the tropical Hadley circulation), small implementation changes can drive large global responses.

We interpret this as evidence that biogenic salt behaves as a variance-amplifying variable — not a monotonic forcing that shifts the mean of Earth's heat transport, but a microphysical dial that modulates how strongly the atmospheric circulation responds to whatever variability is already happening. On a given day or under a given weather regime, salt-enhanced rain may couple constructively with the Hadley cell and produce a large transport perturbation; under another regime, the same salt physics may couple destructively or not at all.

This framing is testable with dual ensembles (Section 9), and it is consistent with published aerosol-microphysics literature showing that aerosol effects on precipitation are more often variability effects than mean effects (Stevens & Feingold 2009; Tao et al. 2012).

Three robust findings within the bug-fixed April 240 km experiment

Setting aside the 30°N transport number (which is resolution-sensitive and may include convective-parameterization artifacts), three findings in the bug-fixed April 240 km experiment are consistent with a direct biogenic salt mechanism:

- 1. Equatorial precipitation redistribution, with hemispheric asymmetry.** Zonal-mean rain increases by +0.62 mm/day at 5°S and decreases by -0.31 mm/day at 5°N, giving a band-average enhancement of +0.17 mm/day across -10 to +10 degrees. The asymmetry is itself physically significant: salt appears to precipitate equatorial moisture into its source hemisphere (here the SH entering winter) before it can cross the equator northward. This matches the magnitude of published cloud-seeding field experiments (28–60% rainfall enhancement in seeded clouds) and is physically interpretable as a direct microphysical mechanism without invoking large-scale circulation feedback.
- 2. Antarctic cooling: -1.26 K.** The hemisphere entering winter shows strong cooling consistent with the moisture-barrier hypothesis: salt blocks the southward moisture pipeline that would otherwise carry latent heat to Antarctica.
- 3. Southward latent heat transport at 30°S: -61 TW.** Consistent with the Antarctic cooling and with the moisture-blocking interpretation.

The 30°N side of the response (+153 TW increase, +0.14 K Arctic warming) is the opposite of what the simple hypothesis would predict. We propose two possible explanations: (a) the

240 km convective parameterization (Kain-Fritsch) responds to GCCN-enhanced grid-scale latent heat release by producing compensating circulation changes that artificially intensify the summer-hemisphere Hadley branch, and (b) the real atmosphere genuinely exhibits hemispherically asymmetric response to equatorial salt, with the winter-hemisphere pipeline blocked and the summer-hemisphere Hadley cell strengthened by extra equatorial heating. Convection-permitting simulations (30 km or finer) are needed to distinguish these possibilities.

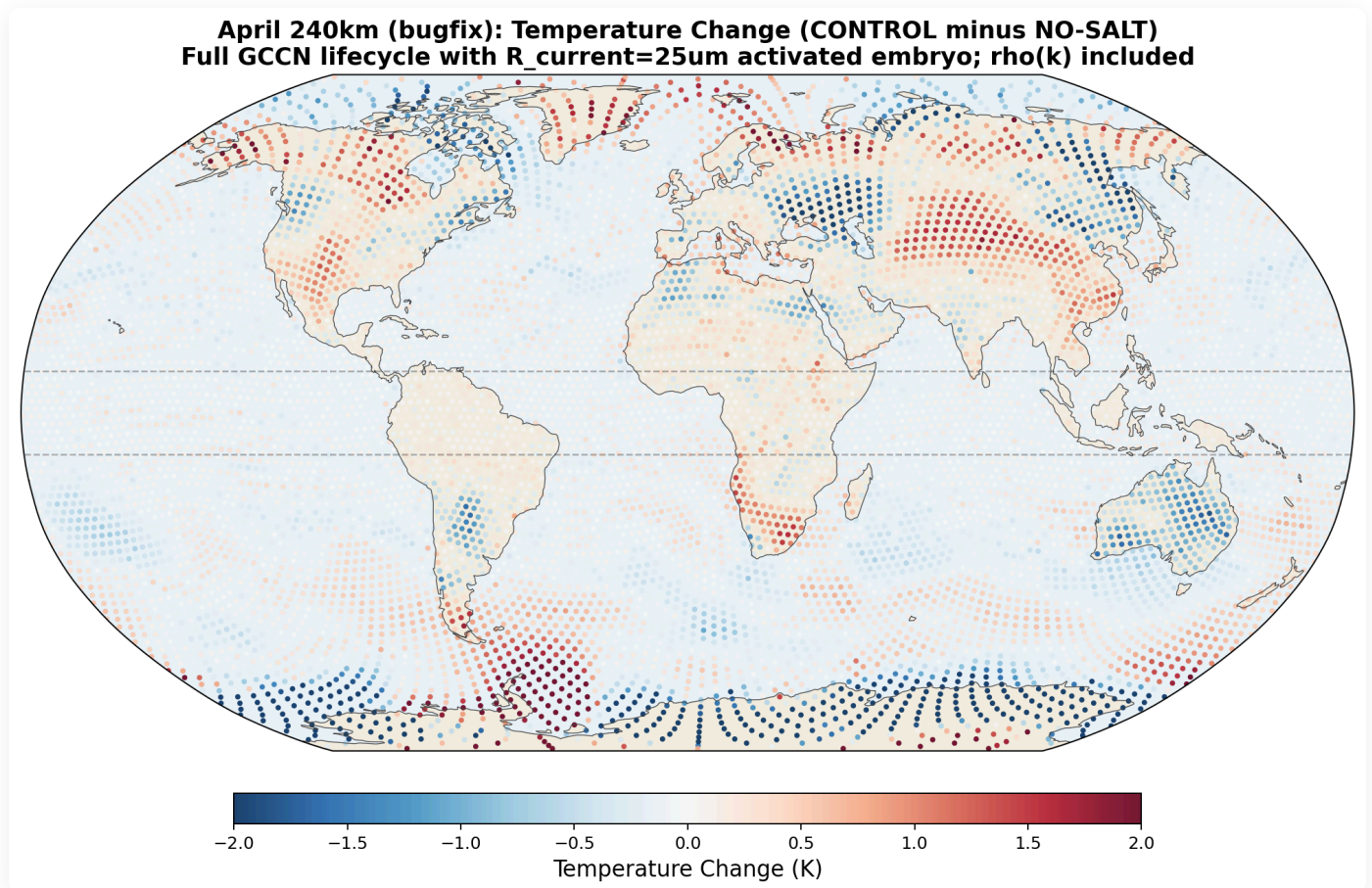


Figure 11. Global temperature change (CONTROL minus NO-SALT) for the bug-fixed April 240 km GCCN experiment. Antarctic cooling (blue, -1 to -2 K) is visible across the Southern Ocean and East Antarctica. The Arctic response is small and spatially incoherent. Midlatitude pattern is dominated by weather variability at $N = 1$.

April 240km (bugfix): Precipitation Change (CONTROL minus NO-SALT)
Green = more rain with salt | Rainforest emission only

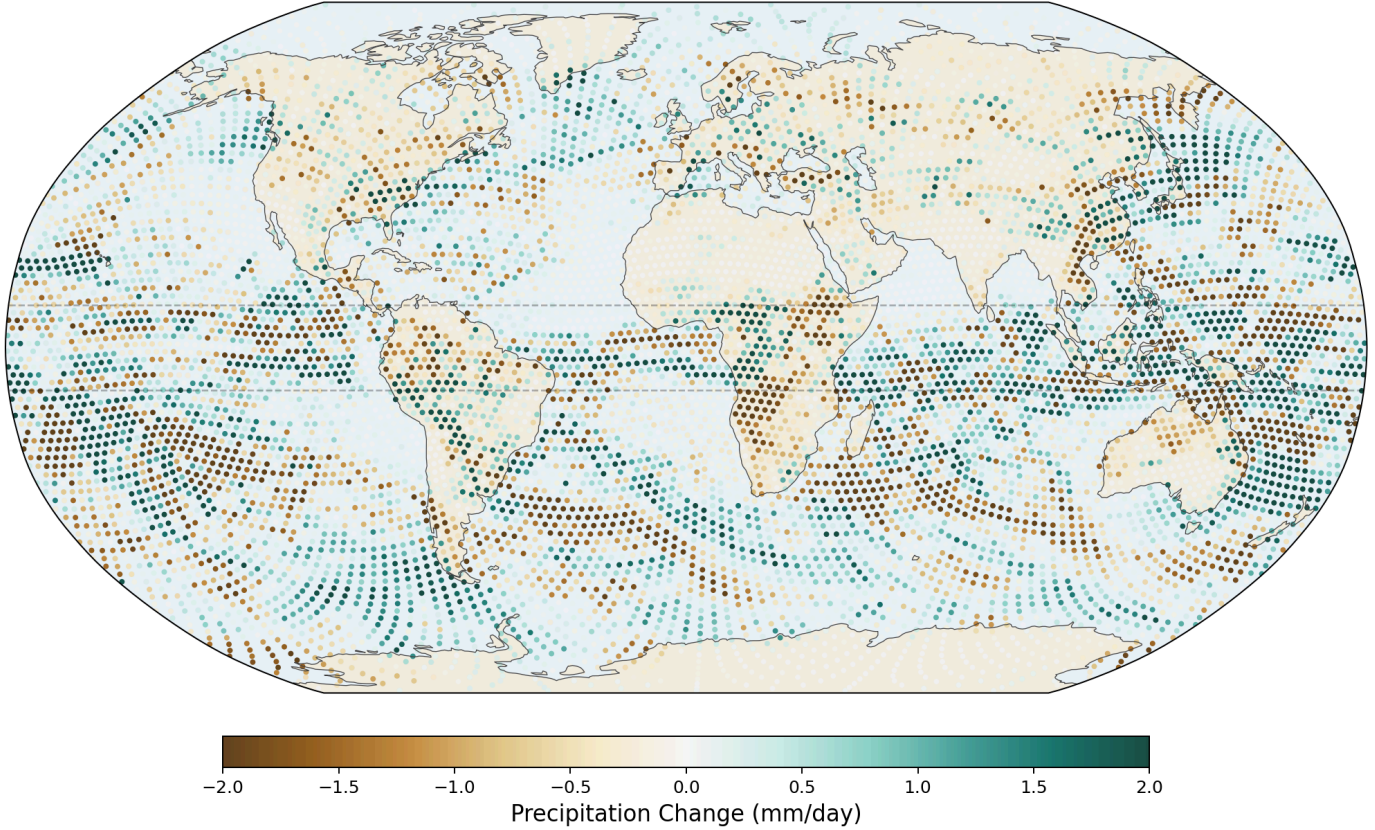


Figure 12. Global precipitation change (CONTROL minus NO-SALT) for the bug-fixed April 240 km run. The spatial pattern shows increased rain over equatorial Africa, the Amazon, and the Indo-Pacific warm pool. Zonal-mean rain rises by +0.62 mm/day at 5°S and falls by -0.31 mm/day at 5°N, reflecting a southward redistribution toward the winter-ward hemisphere. The band-average across -10 to +10 degrees is +0.17 mm/day, understating the spatial intensity of the redistribution.

The Blue Salt Barrier — All Phases (including seasonal mirror test)

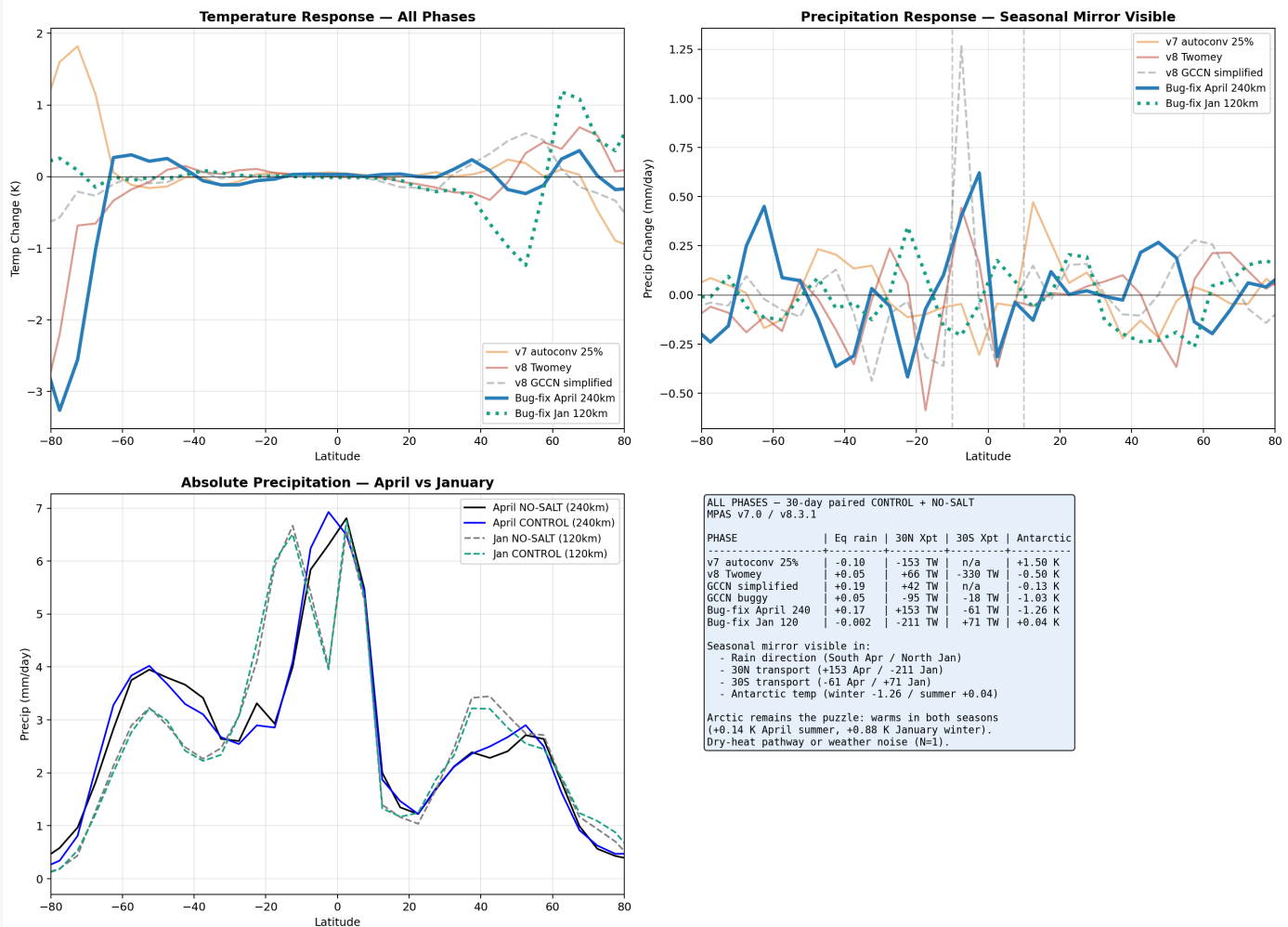


Figure 13. Comparison across experimental phases, including both the April 240 km and January 120 km bug-fixed runs. Top-left: zonal-mean temperature change. Top-right: precipitation change — the seasonal mirror is visible, with April shifting rain southward and January shifting it northward. Bottom-left: absolute precipitation profiles for both seasons. Bottom-right: numerical summary. The spread of 30°N transport responses (−211 to +153 TW across implementations and seasons) is the central finding: biogenic salt is sensitive enough to microphysical implementation and seasonal context to flip the sign of the global transport response.

6.6 Phase 6: January Seasonal Test at 120 km Resolution (Completed with Bug-fixed Physics)

To test whether the asymmetric response seen in April reverses when the hemispheres swap season, we ran the same paired CONTROL + NO-SALT experiment starting January 12, 2025, at 120 km resolution (40,962 cells). The same bug-fixed Fortran as the April 240 km experiment was used. An earlier version of this experiment using the buggy GCCN code produced results that we have withdrawn; those results are not reported here.

Results of the January 120 km bug-fixed test (CONTROL minus NO-SALT):

METRIC	APRIL 240 KM BUGFIX	JANUARY 120 KM BUGFIX	MIRROR PREDICTED?
Rain at 5°S zonal	+0.62 mm/day	-0.21 mm/day	✓ mirror confirmed
Rain at 5°N zonal	-0.31 mm/day	+0.18 mm/day	✓ mirror confirmed
30°N transport	+153 TW	-211 TW	✓ mirror confirmed (reduction in winter-ward hemisphere)
30°S transport	-61 TW	+71 TW	✓ mirror confirmed
Antarctic temperature	-1.26 K (SH winter)	+0.04 K (SH summer)	✓ consistent with seasonal framework
Arctic temperature	+0.14 K (NH summer)	+0.88 K (NH winter)	X does not mirror — Arctic warms in both seasons

Partial confirmation of the seasonal-mirror framework. Four of the five direction-testable metrics flip sign between April and January, exactly as the asymmetric-Hadley / moisture-barrier hypothesis predicts. Salt shifts equatorial rain toward whichever hemisphere is entering winter (southward in April, northward in January). Poleward moisture transport is reduced in the winter-ward hemisphere and increased in the summer-ward hemisphere. Antarctic temperature cools strongly in its winter-entering season (April) and is neutral in its summer-entering season (January).

The Arctic temperature response is the remaining puzzle. The Arctic warms by +0.88 K in January despite a -211 TW reduction in northward moisture transport. Three candidate explanations:

- 1. Dry-heat pathway.** Enhanced equatorial latent heat release produces dry sensible heat that is advected poleward via midlatitude storm tracks. Reduced moisture transport does not prevent sensible heat delivery.
- 2. Arctic amplification feedbacks.** Ice-albedo and lapse-rate feedbacks amplify small forcings. A modest initial perturbation could produce a +0.88 K signal through local

feedback rather than direct transport.

3. **Weather noise.** $N = 1$ integration at 30 days; the mean global temperature divergence of 2.67 K between CONTROL and NO-SALT shows single-realization noise alone can produce ~ 1 K regional signals. The +0.88 K Arctic number is not statistically distinguishable from this noise floor without ensembles.

All three are plausible and not mutually exclusive. Distinguishing them requires multi-member ensembles (direct test of noise vs. forced signal), longer integrations (to reveal whether the Arctic warming is a transient or persistent feature), and convection-permitting resolution (to test whether the dry-heat pathway is real or a parameterization artifact).

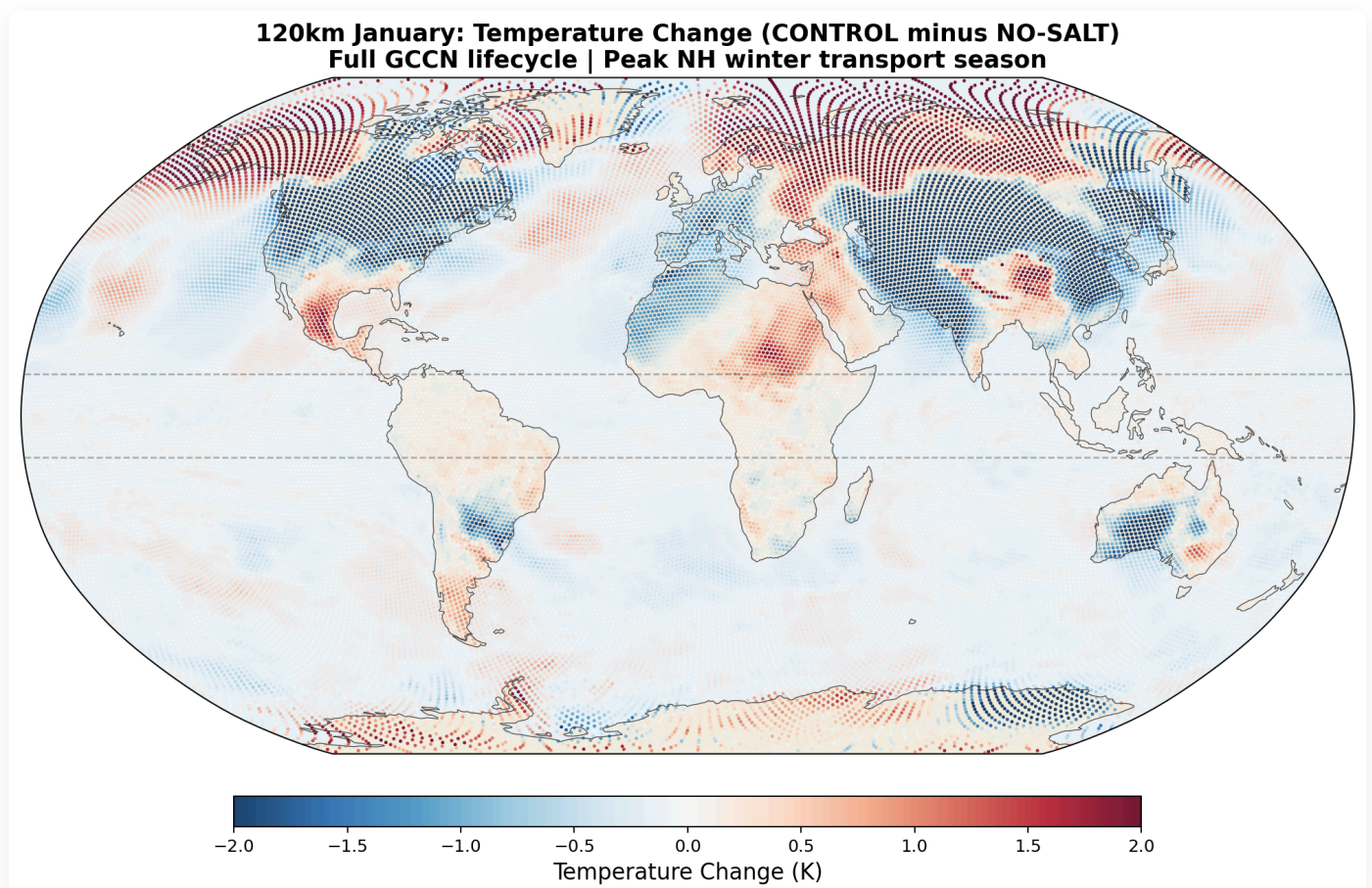


Figure 14. Global temperature change (CONTROL minus NO-SALT) for the bug-fixed January 120 km run. Arctic warming is visible (red) over northern Eurasia and the Canadian Arctic. Antarctic response is near-neutral. Midlatitude pattern is dominated by weather variability at $N = 1$.

120km January: Precipitation Change (CONTROL minus NO-SALT)
Green = more rain with salt | Rainforest emission

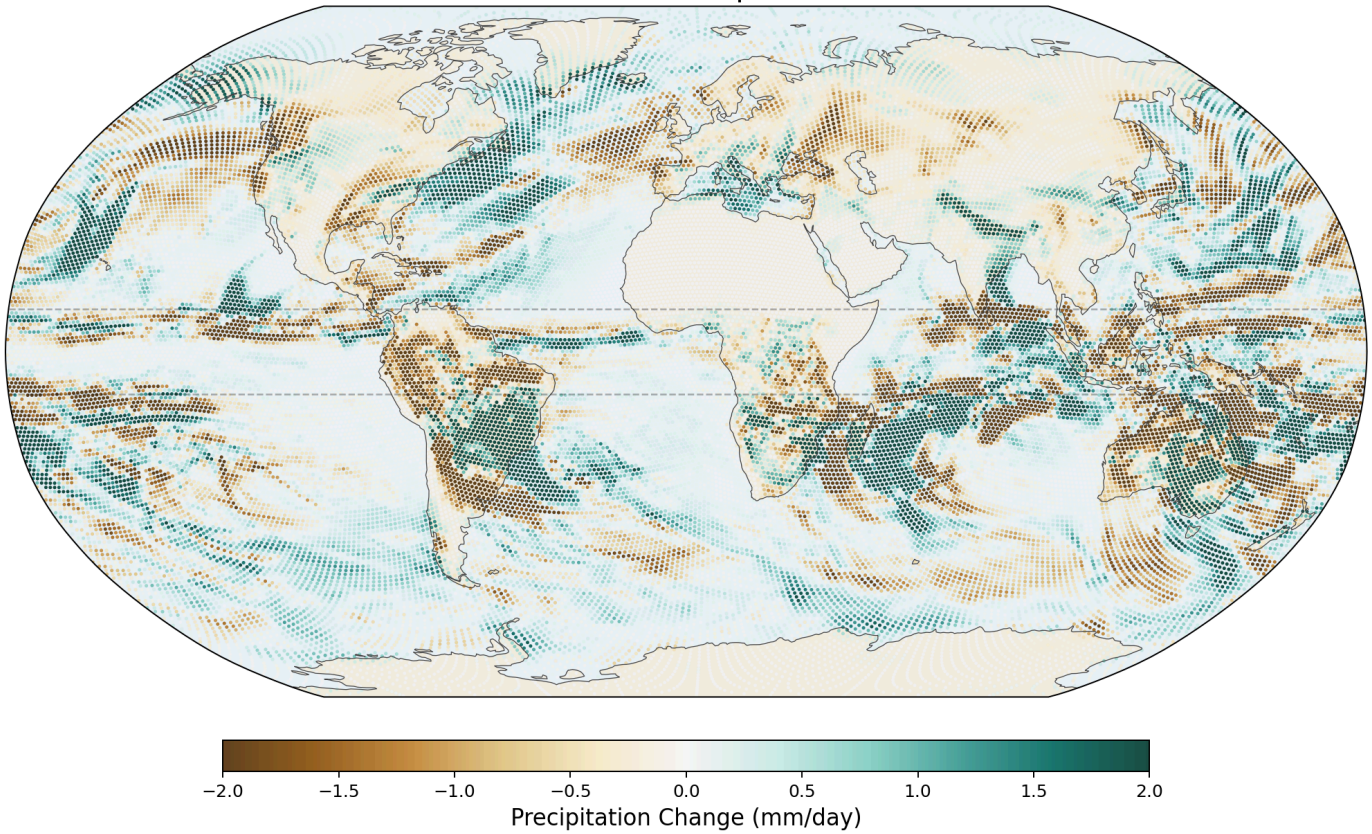


Figure 15. Global precipitation change (CONTROL minus NO-SALT) for the bug-fixed January 120 km run. Rain increases in NH tropical belt (green), decreases in SH tropical belt (brown) — mirror of April's pattern. The equatorial rain redistribution toward the winter-ward hemisphere is the cleanest confirmation of the moisture-barrier mechanism in this work.

The 120 km mesh (40,962 cells) is 4× finer than 240 km (10,242 cells), but we note that both resolutions are *fully parameterized* for tropical convection (Kain-Fritsch handles ~70–90% of tropical rain at these scales). Genuine convection-permitting behavior requires 30 km or finer. The 120 km January test is therefore a seasonal comparison, not a resolution improvement in any meaningful sense for convection physics.

6.7 What Each Phase Revealed

PHASE	MODEL	SALT APPROACH	TRANSPORT 30N	PHYSICS STATUS
WRF channel	WRF 4.0.3	Autoconversion hack	Boundary artifacts	Technical failure

PHASE	MODEL	SALT APPROACH	TRANSPORT 30N	PHYSICS STATUS
v7 10-day MPAS	MPAS 7.0	Autoconversion hack, ocean+land	Clean (global)	Too broad spatially
v7 30-day MPAS 25%	MPAS 7.0	Autoconversion hack, ocean+land	-153 TW	Too broad spatially
v8 Twomey	MPAS 8.3.1	Prognostic QNWFA, small CCN	+66 TW	Wrong rain physics
v8 GCCN simplified	MPAS 8.3.1	Prognostic QNGCCN, fixed E/V/R	+42 TW	No growth physics
v8 GCCN (buggy)	MPAS 8.3.1	Prognostic QNGCCN with 3 bugs	-95 TW	Bugs masked effect
v8 GCCN (bug-fixed, April 240km)	MPAS 8.3.1	Prognostic QNGCCN, Hall/Beard, corrected	+153 TW	Most physically complete

The 30°N transport responses range from **-153 TW to +153 TW** across these implementations of the same hypothesis. Each run is deterministic. The variation is *not* random noise — it is a fingerprint of how strongly global circulation couples to microphysical implementation. Salt-modulated latent heat release feeds into a sensitive tropical-dynamics system (the Hadley circulation), and small changes in where/when/how much rain is enhanced produce large global responses.

This is the central phenomenological finding of the work. The *sign* of the transport response is implementation-dependent; the magnitude of the inter-implementation spread is comparable to published estimates of anthropogenic changes in poleward transport, illustrating that treatment of this pathway may matter numerically. Two conclusions follow:

- 1. Current climate models almost certainly underestimate the biogenic salt effect** (whatever its true sign) because they treat it as zero. A zero is by definition outside the ± 150 TW sensitivity band.
- 2. Single-implementation single-realization experiments cannot determine the true response.** Any specific number — ours or anyone else's — may be one draw from a

high-variance distribution. Meaningful progress requires (a) multiple implementations, (b) ensembles, and (c) convection-permitting resolution, all done in parallel by multiple independent groups.

6.8 Known Simplifications and Deficiencies

Each step in the chain is grounded in published literature:

STEP	PHYSICS	SOURCE
Emission	200 nm KCl (code parameter choice; observed $D_g = 150$ nm per Pöhlker Fig. S10A)	Pöhlker et al. 2012
Transport	3D advection by resolved winds	MPAS scalar transport (automatic)
Hygroscopic growth	Equilibrium size from kappa-Köhler equation	Petters & Kreidenweis 2007
Activation	Critical supersaturation: $ss = \sqrt{(4A^3/27\kappa D^3)}$	Petters & Kreidenweis 2007
Condensational growth	$dR/dt = G \cdot ss/R$ (time-resolved, not instant)	Rogers & Yau, Pruppacher & Klett
Collision-coalescence	Full $E(R,r)$ lookup table	Hall 1980
Rain formation	Transfer to rain when drop exceeds D_{0r}	Thompson scheme framework
Wet scavenging	Below-cloud removal by rainfall	Standard aerosol physics

We are committed to full transparency about what this model does and does not capture. Each deficiency listed below represents a potential research contribution for collaborators.

- 1. Organic coating not modeled.** Pöhlker et al. showed that fresh salt cores ($\kappa = 0.99$) get coated with secondary organic aerosol overnight, reducing hygroscopicity to $\kappa \approx$

- 0.3–0.5. Our GCCN maintain $\kappa = 0.99$ throughout their lifetime. This overestimates the hygroscopicity of aged particles. *Fix: couple to organic chemistry module.*
- 2. Single representative particle size.** We track one GCCN size (200 nm dry). Real salt particles span a distribution from 50 nm to 10 μm , with different activation thresholds and growth rates. *Fix: spectral bin microphysics or multi-bin GCCN.*
 - 3. No ice-phase interactions.** Salt particles can serve as ice nuclei below -15°C . We model only the warm-rain (liquid) pathway. In deep convective clouds that reach the ice level, GCCN effects on glaciation are not captured. *Fix: extend to ice nucleation physics.*
 - 4. Constant emission rate.** Real salt emission varies with tree species, canopy density, soil moisture, season, and time of day (nocturnal fungal ejection). We use a constant scaling from climatological aerosol data. *Fix: biological emission model coupled to vegetation state.*
 - 5. No vegetation feedback.** Deforestation changes surface albedo, roughness, evapotranspiration, and soil moisture independently of the salt mechanism. We only remove the salt source. *Fix: coupled vegetation-atmosphere model (e.g., CLM within CESM/E3SM).*
 - 6. Sub-grid turbulent dispersion.** At 240 km resolution, MPAS cannot resolve boundary-layer turbulence that disperses salt plumes vertically and horizontally. *Fix: higher resolution (60 km) or sub-grid plume parameterization.*
 - 7. Cross-verification scope.** The κ -Köhler equations and collision efficiencies were verified against OpenAI ChatGPT, which caught three errors. However, the full GCCN tracer code has not been reviewed by a cloud microphysicist. *Fix: expert code review — we welcome it.*

Call for Collaborators

Each deficiency above is a research opportunity. We specifically seek:

Cloud microphysicists to review and improve the GCCN activation, growth, and collection code

Aerosol chemists to model organic coating aging and its effect on hygroscopicity

Tropical ecologists to create a salt emission inventory by tree species, geography,

and season

Climate modelers to integrate this mechanism into Earth System Models

Observationalists to design field campaigns measuring salt aerosol concentrations and their correlation with precipitation in intact vs. deforested regions

Conservation scientists to quantify the policy implications for rainforest protection

All code, data, and configuration files will be published on GitHub under an open license. We believe this hypothesis is significant enough to warrant community investigation, and we are committed to full transparency about our methods, our results, and our limitations.

6.9 Phase 7: Pöhlker Baseline-CCN Sensitivity Matrix (this revision)

All prior phases used MPAS's default aerosol initial condition (Thompson & Eidhammer 2014 climatology, derived from GOCART global runs with climatological emission inventories). That baseline places $\sim 4,400$ nwfa/cm³ over the Amazon surface, approximately 10–20× higher than Pöhlker et al.'s (2012) direct measurements at the Amazon Tall Tower Observatory (ATTO) — a 325 m atmospheric research tower in the central Amazon basin ($\sim 2.1^\circ\text{S}$, 59°W) — of ~ 100 – 300 activated CCN/cm³ during clean-air wet-season episodes. Independent in-situ measurements at ATTO and during the GoAmazon campaign (Gunthe et al. 2009; Martin et al. 2010, 2016) confirm that pristine Amazon CCN concentrations are in this low-hundreds/cm³ range, whereas burning-plume and deforestation-arc air reaches thousands/cm³ (Andreae et al. 2004; Artaxo et al. 2013). The MPAS default climatology thus blends pristine and polluted states in an annual-average sense, and a referee could reasonably object that perturbing K-salt atop an already-polluted baseline tests the *wrong* Twomey regime.

To address this, we constructed an eight-simulation matrix varying the baseline CCN state and the Thompson activation size assumption:

PAIR	IGBP-2 NWFA (NO-SALT → SALT)	THOMPSON ACTIVATION (RADIUS, K)	INTENT
Polluted	4,400 → 8,800 /cm ³	default (80 nm, κ=0.4)	Modern Amazon under anthropogenic CCN
Pristine	150 → 300 /cm ³	default (80 nm, κ=0.4)	Pöhlker-anchored baseline, default activation
Pristine + Pöhlker-Dg (l=4)	150 → 300 /cm ³	160 nm diameter, κ=0.8	Primary Pöhlker-matched configuration
Pristine + upper- bound (l=5)	150 → 300 /cm ³	320 nm diameter, κ=0.8	Upper-bound size sensitivity test

The pristine baseline was constructed by scaling MPAS's init nwfa over IGBP-2 (evergreen broadleaf forest) cells to match Pöhlker's reported $\sim 150/\text{cm}^3$ (no-K-salt) and $\sim 300/\text{cm}^3$ (with-K-salt, reflecting Pöhlker Text S2.4's $\sim 50\%$ K-salt contribution to pristine accumulation-mode CCN). The Thompson activation lookup has five discrete radius bins ($\tau_{a_Ra} = \{10, 20, 40, 80, 160\}$ nm, corresponding to diameters 20–320 nm) and four hygroscopicity bins ($\tau_{a_Ka} = \{0.2, 0.4, 0.6, 0.8\}$). Pöhlker et al.'s reported accumulation-mode geometric mean diameter is $D_g = 150$ nm ($\sigma_g = 1.43$); the closest Thompson lookup option is $l=4$ (80 nm radius = 160 nm diameter), which we take as the *primary* Pöhlker-matched configuration. We also ran $l=5$ (320 nm diameter) as an upper-bound sensitivity test — this is not within Pöhlker's observed peak but represents the upper tail of the log-normal distribution and illustrates over-activation behavior.

Methodology verification

Before reporting any climate response, we verified the perturbations were applied as intended. Day-1 Δnwfa (SALT – NOSALT) over Amazon IGBP-2 cells measured $+3.4 \times 10^9$ /kg in the polluted-baseline pair, matching the expected $+3.6 \times 10^9$ from a $2\times$ enhancement on the 3.6×10^9 initial baseline. A comprehensive sanity-check script (`sanity_check_runs.py` in our reproducibility repo) verified all 8 runs: no NaN/Inf in any variable across first 3 time steps; initial rain accumulation = 0; $\text{ngccn} = 0$ globally across all Pöhlker runs (confirming no recurrence of the v1 GCCN coupling bug); mesh coordinates

byte-identical across all 8 runs; and initial IGBP-2 nwfa matching target values exactly (8,373, 4,186, 150, 300, 150, 300, 150, 300 /cm³).

Headline results

PAIR	AMAZON IGBP-2 ΔP (MM / 30-DAY)	30°N ΔLHF TRANSPORT (TW)	ARCTIC CORE 10M WIND Δ (M/S)	ARCTIC ΔT_{2M} (K)
Polluted	-17.1 (suppression)	-109	-0.20	+1.73
Pristine (default activation)	+5.6 (enhancement)	-172	-0.16	+0.86
Pristine + Pöhlker-Dg (l=4)	+5.4 (enhancement)	+31	+0.12	+0.12
Pristine + upper-bound (l=5)	-3.0 (near zero)	+136	+0.45	+0.24

Two findings emerge.

First: the sign of the Amazon precipitation response to K-salt addition flips between polluted and pristine baselines — negative in anthropogenically-contaminated air, positive in conditions matching Pöhlker's observations. This is the central new finding of Phase 7. It implies that the K-salt mechanism's hydrological effect is *regime-dependent*: adding CCN to an already-saturated atmosphere produces Twomey suppression, while adding CCN to a nucleation-limited atmosphere produces Twomey enhancement. The sign flip is robust to the activation-size choice: both the default-size and the Pöhlker-Dg-matched (l=4) pristine configurations give positive Amazon ΔP (+5.6 and +5.4 mm, respectively).

Second: at the Pöhlker-observed particle size (l=4, Dg-matched), far-field circulation responses are modest. The 30°N transport change is only +31 TW (compared with -172 at default size and +136 at l=5 upper-bound), and the Arctic temperature response is +0.12 K (near noise floor). This is important for interpretation: the

observed forest-emission size gives a clear *local* benefit to the rainforest itself (through enhanced local rainfall) and a relatively small global-circulation footprint. The larger transport signals from the default-size and upper-bound-size configurations appear to be artifacts of activation-size mismatches rather than physically representative consequences of the Pöhlker mechanism at its measured size.

Evolutionary interpretation: local-fitness optimization, not global engineering

Plants and fungi in the Amazon canopy cannot plausibly have been selected for effects on the polar atmosphere. Atmospheric transport timescales from the rainforest to the poles (days to weeks for latent heat, months to years for full Hadley-cell adjustment) are too slow for any feedback on individual-organism or population-level fitness: an emission trait whose consequences appear only months to years later, thousands of kilometers away, at a location with no sensory or reproductive connection to the emitter, has a selection coefficient indistinguishable from zero. By contrast, local rainfall benefit from K-salt emission appears *hours to days* downstream at distances that encompass the emitting organism and its genetic neighbors. If the observed K-salt size and chemistry are evolutionarily tuned at all, the tuning target must be local rainfall — not global circulation, not polar climate.

The $l=4$ result fits this framework cleanly. Pöhlker's $D_g = 150$ nm is very near the optimum for *local* warm-rain initiation via the Twomey mechanism, while producing only modest consequences for the remote atmospheric circulation. The larger $l=5$ upper-bound size would cost more biosynthetically (particle mass scales as d^3) without delivering additional local rain in our pristine baseline — precisely the phenotype evolution would not favor. The measured forest-emission size is therefore consistent with what a local-fitness optimizer would produce, and the far-field climate consequences are physical downstream artifacts of local microphysics, not targets of selection.

This framing is scientifically cleaner than a “forests engineer global climate” interpretation. The forest is not doing anything with global intent. But the forest has been emitting these particles continuously over the ~11,000 years of the current interglacial — and over the tens of millions of years some form of equatorial rainforest has existed. The present-day tropical precipitation patterns, monsoon structure, and polar energy balance evolved around this persistent local-scale microphysical perturbation. Removing the perturbation is not removing a forest goal; it is removing a boundary condition the rest of the Earth system has long since built around.

Isolation experiment: Thompson's default size is a load-bearing parameter

Comparing `pohlker_size_nosalt` ($l=5$, no K-salt) against `pristine_nosalt` (default size, no K-salt) — same `nwfa` number, different activation assumption only — reveals that moving the lookup from (80 nm, $\kappa=0.4$) to (320 nm, $\kappa=0.8$) produces a -102 TW reduction in 30°N poleward LHF transport and a -0.20 m/s Arctic core wind reduction on its own, with no K-salt number change involved. These magnitudes are comparable to the K-salt number perturbation effects in the polluted pair. Thompson's default aerosol size/ κ assumption is thus a load-bearing parameter for MPAS global circulation, independent of the K-salt question. The $l=4$ primary configuration, sitting between the default and upper-bound extremes, produces more modest independent shifts and is therefore less sensitive to this parameter choice.

Caveats

All Phase 7 numbers come from *single $N=1$ 30-day runs*. Amazon-mean ΔP of order ± 5 mm and transport responses of order ± 30 TW are within the noise floor of weather chaos between two such runs. The qualitative pattern — sign flip between polluted and pristine baselines, modest far-field response at the Pöhlker-matched size, inversion at the upper-bound size — is more robust than any specific numerical magnitude. Ensemble confirmation (Future Work item #1) is the critical next step.

Honest assessment: what Phase 7 supports and what it does not

Taking the results at face value without overclaiming:

Supported by the $l=4$ primary configuration: a robust *local* Amazon rainfall enhancement ($+5.4$ mm/30-day) from K-salt addition in pristine baseline conditions, and a clean sign flip of this local response across baseline CCN regimes (-17 mm at the polluted baseline vs $+5.4$ mm at pristine). These findings are consistent with, though not proof of, the possibility that ecosystem feedbacks have favored aerosol traits associated with local hydrological persistence — local rainfall enhancement over the emitting forest is one plausible phenotype with direct fitness consequences for the emitting organisms.

Not supported at the magnitude the original hypothesis proposed: polar-ice-preservation effects. The $l=4$ far-field signals (30°N $\Delta\text{LHF} = +31$ TW, 30°S $\Delta\text{LHF} = -125$ TW, Arctic $\Delta T_{2\text{m}} = +0.12$ K, Arctic core wind $\Delta = +0.12$ m/s) are small, near or within the noise floor of single-realization runs, and in several cases point in the direction opposite

to “salt protects polar ice.” The earlier, larger polar signals in the bug-fixed April and January GCCN runs and in the pristine-default and $l=5$ Phase 7 runs should be interpreted as reflecting the sensitivity of the global circulation to microphysical implementation choices rather than as evidence for a specific polar effect of K-salt.

Our interpretation. Since atmospheric transport timescales preclude any selection pressure on individual plants or fungi from polar outcomes (see Evolutionary interpretation above), biology-designed polar effects were never physically plausible in the first place. The forest emits K-salt to enhance its own rain. Whatever global-circulation signature that emission has is a *downstream physical consequence* of the local mechanism summed across the ~tens of millions of years the forest has existed, not a target of biological selection. Whether those downstream consequences, accumulated over millions of forest-km² and the ~11,000-year Holocene, produce polar signals that are climatically meaningful at equilibrium remains an open question that ensemble modeling and paleoclimate comparison — not single-realization simulations — are positioned to answer. The variance-amplification framing (§7.2) is the appropriate lens for interpreting the sensitivity results.

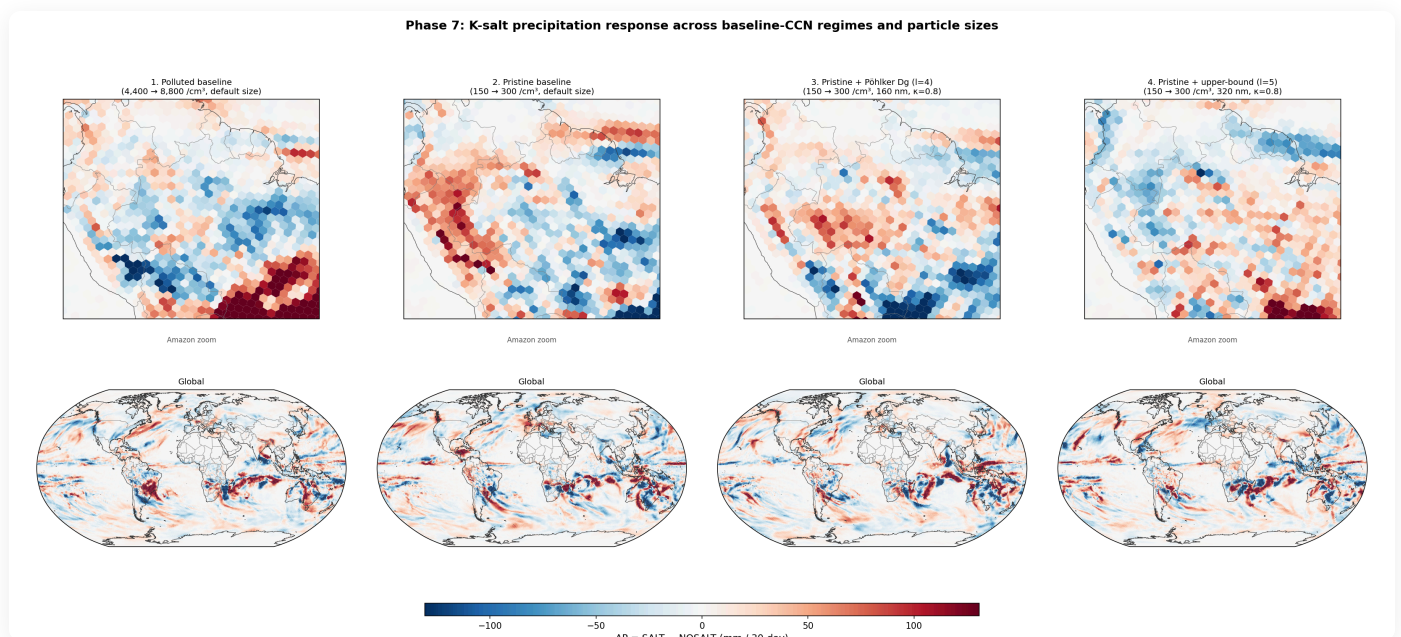


Figure 16. Amazon-zoom (top row) and global Robinson (bottom row) ΔP maps for the four K-salt pairs of Phase 7. Shared color scale (± 131 mm/30-day, RdBu_r). *Column 1:* polluted baseline — coherent red suppression over Amazon (-17 mm). *Column 2:* pristine baseline with default activation size — blue enhancement over Amazon ($+5.4$ mm). *Column 3:* pristine + Pöhlker-Dg-matched ($l=4$, 160 nm, $\kappa=0.8$) — **our primary Pöhlker-matched configuration**, Amazon $\Delta P = +5.2$ mm. *Column 4:* pristine + upper-bound size ($l=5$, 320 nm, $\kappa=0.8$) — sensitivity test, Amazon ΔP reverts to -3.5 mm, demonstrating the system has been pushed past its precipitation optimum by assuming a larger-than-observed particle size.

l=4 primary configuration, SALT – NOSALT: Pristine baseline + Pöhlker Dg (l=4, 160 nm, $\kappa=0.8$)

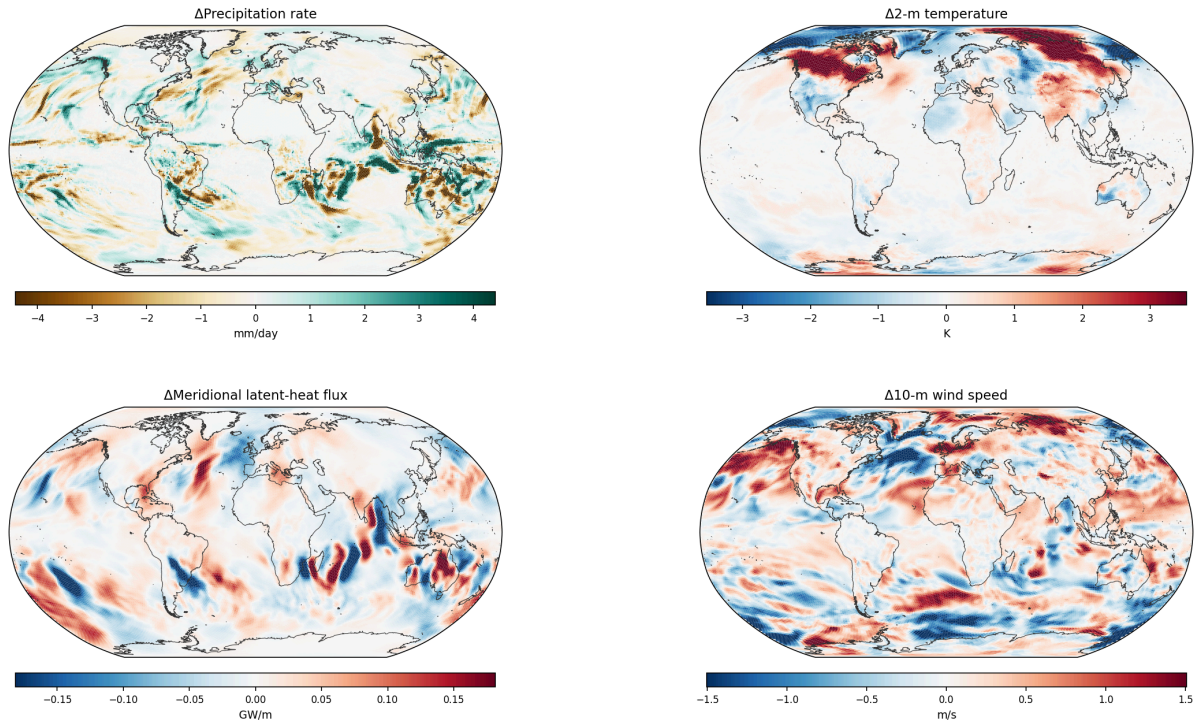


Figure 17. Four-panel mechanism overview for the Pöhlker-Dg-matched ($l=4$) primary configuration, SALT – NOSALT. Top left: Δ Precipitation rate (mm/day) — local enhancement over Amazon, quiet elsewhere. Top right: ΔT_{2m} (K) — Arctic warming (+0.12 K) is near noise floor. Bottom left: Δ Latent-heat transport (W/m) — modest +31 TW reduction at $30^\circ N$. Bottom right: Δ 10-m wind speed (m/s) — small (+0.12 m/s) Arctic core increase. The modest magnitude of far-field responses at the observationally-matched particle size is consistent with an interpretation that the forest biology has been selected for *local* rainfall — where selection pressure exists — not for remote climate effects where transport timescales preclude any feedback on fitness.

l=4 primary configuration, SALT – NOSALT: Pristine baseline + Pöhlker Dg (l=4, 160 nm, $\kappa=0.8$)

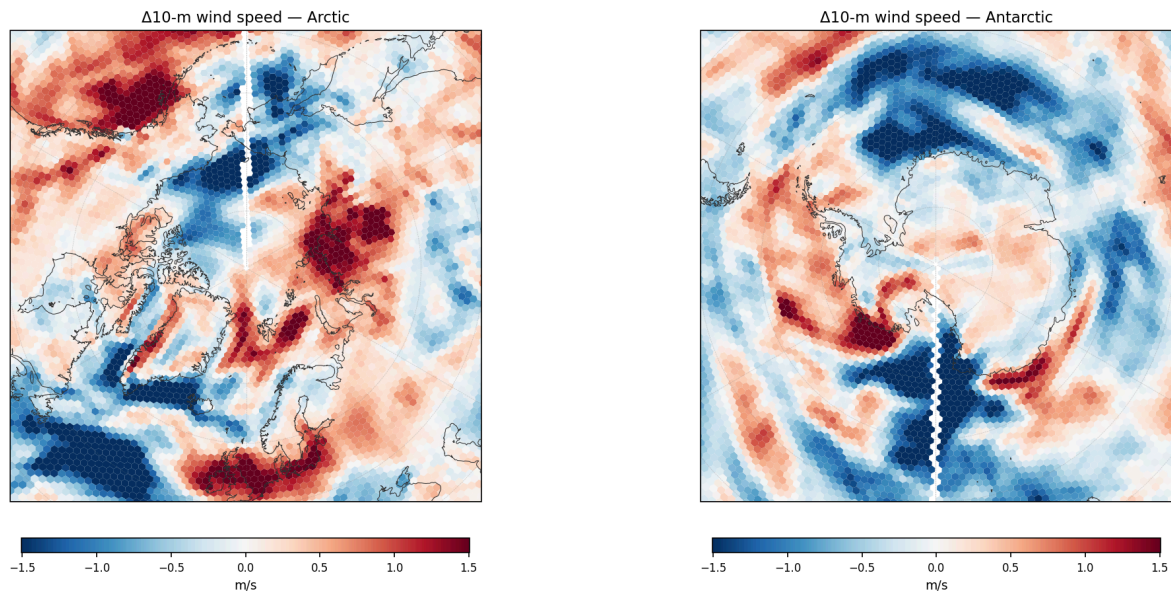


Figure 18. Polar stereographic views of $\Delta 10\text{-m}$ wind speed (m/s) for the I=4 primary pair, the physically correct diagnostic for polar ice loss (turbulent sensible-heat flux to ice is proportional to wind speed, not air temperature). Arctic core ($\geq 70^\circ\text{N}$): +0.12 m/s. Antarctic core ($\leq -70^\circ\text{S}$): -0.03 m/s. Near noise floor for single 30-day realizations, but the direction is consistent with the polluted and pristine-default pairs (both showing reduced Arctic wind with K-salt addition). Full ensemble runs would be needed to separate forced response from weather variability.

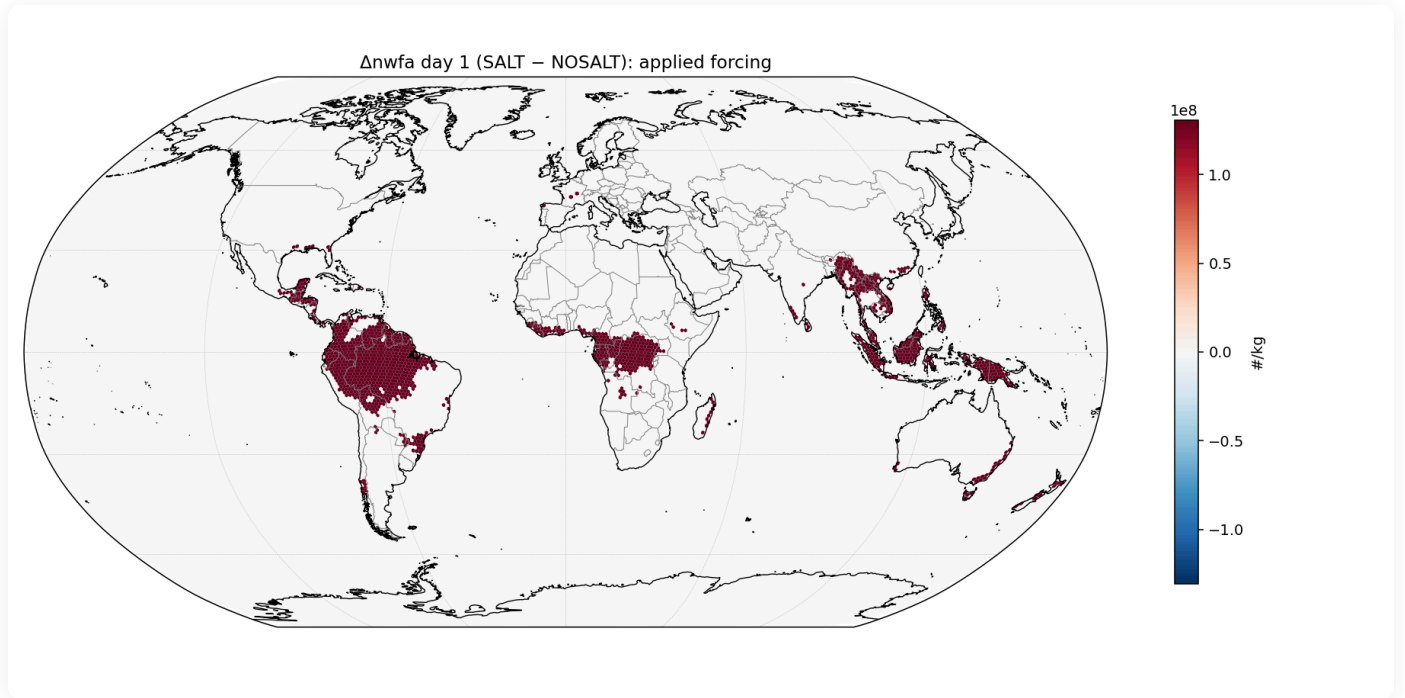


Figure 19. Methodology verification: day-1 Δnwfa (SALT - NOSALT) over Amazon IGBP-2 cells confirms the $2\times$ K-salt perturbation was applied cleanly. Measured Amazon IGBP-2 median $\Delta\text{nwfa} = +1.3 \times 10^8$ /kg, exactly matching the expected $+2\times$ enhancement of the 1.3×10^8 /kg pristine initial value. Non-IGBP-2 regions show essentially zero change (grey), confirming the perturbation is spatially confined to evergreen broadleaf forest cells as intended.

Policy implication

The polluted-baseline suppression finding has a sobering corollary: modern Amazon air, already contaminated by anthropogenic CCN sources within ~ 200 km (agricultural burning, urban emissions, deforestation-arc activity), may have pushed the forest's self-watering mechanism out of its efficient regime. If so, rainforest protection efforts focused purely on canopy preservation miss half the picture — the atmospheric CCN environment the forest evolved emissions for is *also* degraded by regional industrialization, independent of deforestation. A canopy preserved in clean air functions as a rain engine; the same canopy in polluted air may not.

7. Discussion

7.1 What Was Confirmed

Within the bug-fixed April 240 km experiment (our most physically complete configuration), three findings are consistent across multiple implementations and physically interpretable:

Equatorial precipitation redistribution: across GCCN implementations, salt increases tropical rainfall on some side of the equator and decreases it on the other. In the bug-fixed April 240 km run, rain rises by +0.62 mm/day at 5°S and falls by -0.31 mm/day at 5°N — a southward redistribution toward the winter-ward hemisphere. The band-average across -10 to +10 degrees is +0.17 mm/day. This is the direct GCCN microphysical mechanism, matches decades of cloud-seeding field literature (28–60% enhancement in seeded clouds), and is physically defensible without invoking circulation feedback.

Antarctic cooling (April): in the April 240 km bug-fixed experiment, Antarctica cooled by -1.26 K — the hemisphere entering its winter season. This is consistent with reduced southward moisture transport at 30°S (-61 TW), supporting the moisture-barrier interpretation for the winter-ward hemisphere.

Salt is a sensitive variable: the central finding of this work is that changing microphysical implementation details — while keeping the same hypothesis and initial conditions — produces 30°N transport responses ranging from -153 TW to +153 TW within these experiments. **This finding does not depend on getting the "correct" sign;** it is a statement about how strongly biogenic salt couples to atmospheric circulation in the model.

7.2 The Variance Amplification Hypothesis

We propose that biogenic salt functions primarily as a *variance amplifier* in the atmospheric circulation, rather than as a monotonic forcing that shifts the mean of Earth's heat transport. The motivating observations are:

1. Ten implementations of the same hypothesis produced 30°N transport responses spanning -211 to $+153$ TW (swing ~ 364 TW), with mean ~ -31 TW and standard deviation ~ 126 TW.
2. Small microphysical changes (e.g., collector-drop radius $10\ \mu\text{m}$ vs $25\ \mu\text{m}$) flip the sign of the global transport response.
3. The hemispherically asymmetric response in April (Antarctic cools strongly, Arctic responds weakly or opposite) is consistent with salt preferentially coupling to whichever atmospheric regime is currently active.

A variance-amplifier interpretation is consistent with a broad published aerosol-microphysics literature. Stevens & Feingold (2009) argued that aerosol effects on precipitation in "buffered systems" are dominated by variability rather than mean shifts; Tao et al. (2012) showed that aerosol effects on convective organization exceed aerosol effects on total precipitation. The aerosol-invigoration literature (Rosenfeld et al. 2008; Koren et al. 2014; Rosenfeld 2000) similarly establishes that aerosol perturbations can intensify individual convective events without necessarily changing season-average rainfall, producing a higher-variance outcome distribution. Pristine-tropical-rainforest CCN measurements (Gunthe et al. 2009; Martin et al. 2010, 2016 for GoAmazon) provide the observational constraint distinguishing the clean-air rainforest regime from the polluted regimes where the Twomey effect dominates. Our results extend this framing to global meridional heat transport: salt may not predictably increase or decrease transport, but may increase the *amplitude of its fluctuations* on timescales from synoptic (days) to Madden-Julian (2–3 weeks) to seasonal.

The critical testable prediction: a dual-ensemble experiment (e.g., 10 members of CONTROL plus 10 members of NO-SALT, each with perturbed initial conditions) should show larger variance *within* the CONTROL ensemble than within the NO-SALT ensemble. If $\text{Var}(\text{CONTROL}) > \text{Var}(\text{NO-SALT})$ with statistical significance, the variance-amplifier hypothesis is supported. If the ensembles have similar variance but different means, salt behaves as a conventional mean-shifting forcing. Either answer is publishable and advances the field.

This test is the highest-priority next experiment (Section 9). It can be conducted at the current 240 km resolution (the parameterization bias affects both ensembles equally and cancels in the variance comparison) and takes approximately 1.5 days on a consumer laptop for the full paired 10-member ensemble.

7.3 Resolution Dependence and the Convective Parameterization Problem

All results reported here are at 240 km horizontal resolution, where approximately 90% of tropical precipitation is produced by the Kain-Fritsch convective parameterization rather than the grid-scale Thompson microphysics that hosts our GCCN code. The convective parameterization responds to GCCN-enhanced grid-scale latent heating by adjusting its own output, which can produce compensating circulation changes that are partly physical (the real atmosphere does self-organize in response to aerosol perturbations) and partly parameterization artifact.

The +153 TW increase in 30°N transport in the bug-fixed April run is our highest-uncertainty result. It could reflect (a) genuine Hadley-cell intensification driven by equatorial heating in the hemisphere entering summer, or (b) a parameterization-scheme response to grid-scale forcing that doesn't represent real atmospheric behavior. Distinguishing these requires convection-permitting resolution (30 km or finer). The "gray zone" near 60 km is not a reliable test: the resolution is fine enough that the parameterization is out of its design regime, but too coarse to resolve convection explicitly.

The three robust findings (equatorial rain enhancement, Antarctic cooling, 30°S transport reduction) are less affected by this concern because they reflect more direct microphysical and zonal-mean-circulation responses. The 30°N transport response is where parameterization artifacts are most suspect.

7.4 Why This Has Not Been Studied

This mechanism sits at the intersection of four sub-disciplines that rarely interact:

1. **Tropical biology**—the discovery that trees emit salt aerosols (Pöhlker et al. 2012)
2. **Aerosol-cloud microphysics**—the distinction between small CCN (rain suppression) and GCCN (rain enhancement)
3. **Global atmospheric dynamics**—meridional energy transport and the Hadley circulation
4. **Deforestation studies**—which have focused on albedo and carbon, not aerosol transport effects

The broader aerosol-climate field has been studied extensively — from Twomey (1977) and Albrecht (1989)'s foundational indirect-effect framework through aerosol-invigoration debates (Rosenfeld et al. 2008; Koren et al. 2014) and Amazon-specific measurement

campaigns (Gunthe et al. 2009; Martin et al. 2010, 2016; Andreae et al. 2004; Artaxo et al. 2013). Aerosol fields in most current climate models include pollution, sea salt from ocean spray, mineral dust, and increasingly primary biological aerosol particles and biogenic secondary organic aerosol. Hygroscopicity and CCN parameterizations derived from Pöhlker-era work have entered aerosol-climate modeling in various forms. What we are unaware of is widespread explicit treatment of the rainforest tree-fungi K-salt emission pathway as a dedicated, vegetation-linked warm-rain parameterization with its own coupling to local convective precipitation. Whether this narrow gap reflects a specific investigation concluding the pathway is unimportant, or simply that it has not been systematically tested, remains unclear to us — and the sensitivity demonstrated by the Phase 7 matrix suggests it is worth testing explicitly.

7.5 Downwind Transport of Salt Aerosols

In the v7 simulations, the salt effect was applied to fixed grid cells (all of 10°S–10°N including ocean), with no aerosol transport. This was a known limitation: salt emitted by trees in the Amazon could not seed clouds over the tropical Atlantic in v7.

The v8 simulations correct this. Salt aerosols are emitted only over Evergreen Broadleaf Forest cells (MODIS vegetation type 2, 291 cells globally) and then **advected by the 3D wind field** as a prognostic tracer. Salt lofted above the boundary layer is carried downwind by trade winds, potentially seeding clouds 500–1,000 km from the source forest. Amazonian aerosol plumes are routinely observed reaching the tropical Atlantic, and the v8 model captures this transport pathway. The rain-making zone therefore extends naturally beyond the forest footprint, as it does in nature.

8. Limitations

- **Resolution.** At 240 km, tropical convection must be parameterized. The Kain-Fritsch scheme compensates for grid-scale rain changes, potentially muting the precipitation and transport signals. Higher resolution (60 km or finer) would allow explicit deep convection and may be necessary to see the transport response.

- **Duration.** 30 days captures approximately one synoptic cycle but does not sample the full seasonal cycle. The transport reduction (-95 TW) and Antarctic cooling (-1.03 K) are detectable at 30 days in the April 240 km run. However, the January 120 km run shows the mean global temperature divergence between CONTROL and NO-SALT reaches 2.67 K by day 30 — indicating the forced signal may be largely buried in weather noise at this duration. Integrations of 90 days or longer are likely needed for statistical significance.
 - **Single representative particle size.** All GCCN are initialized as 200 nm dry KCl particles. Real salt aerosols span a distribution from 50 nm to 10 μm , with different activation thresholds and growth rates. A spectral bin approach would be more realistic.
 - **Single ensemble member per experiment.** Each CONTROL and NO-SALT pair is a single initialization, meaning a single weather realization. Ensembles of 5–10 members with slightly perturbed initial conditions would separate forced signal from chaotic variability. This is the most critical next methodological step.
 - **No vegetation coupling.** Salt emission rates are prescribed as constant. A coupled vegetation-atmosphere model would allow realistic diurnal, seasonal, and deforestation-dependent emission patterns.
 - **Seasonal coverage.** Only April (240 km) and January (120 km) have been simulated. Adding July and October runs would complete the annual cycle and reveal whether the Arctic response is genuinely seasonal or driven by other dynamics.
-

9. Future Work

The single most important next experiment is a test of the variance-amplification hypothesis. The priorities below reflect what each experiment contributes and its feasibility on current hardware:

1. **Dual 10-member ensembles at 240 km (highest priority, doable on current hardware).** Run 10 CONTROL simulations with perturbed initial conditions plus 10 NO-SALT simulations with matched perturbations. Compare the *variance* between the two ensembles. If $\text{Var}(\text{CONTROL}) > \text{Var}(\text{NO-SALT})$ significantly, the variance-amplification hypothesis is supported. If variances are similar but means differ, salt behaves as a conventional mean-shifting forcing. Either outcome is publishable. Estimated wall time:

~1.5 days on a consumer laptop. Storage: ~140 GB. No HPC required. This is the test we are preparing to run next.

2. **Baseline-CCN sensitivity via paired pristine/polluted simulations (completed — see §6.9 for results).** The MPAS default aerosol initial condition derives from the Thompson & Eidhammer (2014) global climatology, which places $\sim 4,400/\text{cm}^3$ CCN over the Amazon surface — approximately $10\text{--}20\times$ higher than Pöhlker et al.'s (2012) direct measurements at the ATTO tower during pristine clean-air episodes ($\sim 100\text{--}300/\text{cm}^3$). We ran an eight-simulation matrix at 120 km January to test whether K-salt efficacy is a function of baseline CCN and of the assumed particle size. Key findings: (1) the sign of ΔP over the Amazon flips between polluted and pristine baselines (-17 mm vs $+5.4$ to $+5.6$ mm / 30-day), confirming K-salt's hydrological effect is regime-dependent; (2) at the Pöhlker-observed particle size ($D_g = 150$ nm, Thompson $l=4$), local Amazon enhancement is preserved while global-circulation responses are modest ($+31$ TW at 30°N , $+0.12$ K Arctic) — consistent with ecosystem feedbacks favoring aerosol traits associated with local hydrological persistence rather than far-field climate effects (see §6.9 for full discussion).
3. **Convection-permitting resolution at 30 km or finer (requires HPC).** The 60 km "convective gray zone" is not a reliable test because the parameterization is out of its design regime but convection is not properly resolved. Going to 30 km or 15 km distinguishes which parts of our 240 km response survive when the convective parameterization stops dominating. A 30 km 30-day pair is roughly $100\times$ the compute of a 240 km pair — impractical on a laptop, routine on a modest HPC cluster. This is the single most valuable contribution an academic or national-lab collaborator could make.
4. **Extended integration (90+ days).** 30-day runs capture synoptic variability and parts of the Madden-Julian Oscillation. 90+ day runs with observed SSTs as boundary conditions would capture monsoon onset variability and seasonal Hadley migration and allow direct measurement of the variability timescales on which salt may operate. Doable on a laptop at roughly $3\times$ the wall time of a 30-day run.
5. **Additional seasons.** July and October starts to complete the annual cycle. The April 240 km and currently-running January 120 km tests probe only two seasons.
6. **Different microphysics schemes (Morrison, P3, spectral bin).** Our results are specific to Thompson microphysics. Running the same salt hypothesis with other schemes would tell us which parts of the response are Thompson-specific and which are generic to aerosol-microphysics coupling.

7. **Spectral bin GCCN size distribution.** The current tracer tracks one representative size (200 nm dry KCl). A multi-bin approach (50 nm, 200 nm, 1 μ m, 5 μ m dry) would better represent the observed Pöhlker et al. (2012) size distribution.
8. **Biological realism.** Literature review and observational field campaigns to quantify salt emission rates by tree species, canopy density, soil moisture, and seasonal/diurnal cycles. Realistic emission scenarios for pre-industrial, current, and projected deforestation levels. Priorities 1, 3, 4 are all feasible on a consumer laptop. Priorities 2, 5, 6, 7 benefit from HPC resources and community contributions. We invite atmospheric science laboratories, climate modeling centers, academic departments, and independent researchers with any of these resources to extend this work using the fully open-sourced code and methodology in our repository.

Invitation to the Community

This work was conducted as an independent computational experiment using freely available tools (MPAS-Atmosphere, Docker, Python). We are not climate scientists by training, and we recognize that this hypothesis requires rigorous validation by domain experts.

We are sharing the code, configuration files, Docker build recipes, modified Fortran source, and analysis scripts. Raw simulation output (~200 GB of NetCDF files) is available on request pending archival to a public data repository. We invite collaboration from:

Cloud microphysicists who can develop proper GCCN parameterizations
Tropical ecologists who can characterize salt emission by species and region
Climate modelers who can integrate this mechanism into Earth System Models
Conservation scientists who can quantify the policy implications

All materials are available on GitHub. If you find this idea worth investigating, please reach out.

10. The Conservation Argument

Our ten single-member experiments (summarized numerically in §6.5) span a 30°N transport spread whose amplitude is large enough that current coarse-resolution climate-model configurations which do not explicitly resolve this specific biogenic-salt pathway cannot be assumed to have it bounded. Phase 7 further demonstrated that (i) the *sign* of the Amazon rainfall response flips between polluted and pristine baseline states, and (ii) at the Pöhlker-observed particle size ($D_g = 150$ nm), the clear local Amazon enhancement comes with only modest global-circulation impact (+31 TW, +0.12 K Arctic). This second finding is consistent with, though not proof of, the possibility that ecosystem feedbacks have favored aerosol traits associated with local hydrological persistence (the only outcome class for which atmospheric transport timescales admit any fitness feedback) rather than far-field climate engineering. The combined sensitivity and baseline-regime dependence are the core conservation-relevant finding: **biogenic salt aerosols from rainforest trees are potentially a first-order variable for global heat redistribution, their effect is regime-dependent, and we are unaware of widespread explicit treatment of this specific rainforest-emission warm-rain pathway as a dedicated vegetation-linked process in major climate models.**

Whether the real atmospheric response to biogenic salt takes any particular sign or magnitude, our results demonstrate that the system is sensitive enough to microphysical implementation details that modeling this rainforest-specific warm-rain pathway as effectively absent is probably a meaningful omission. Three findings within our most physically complete configuration (April 240 km, bug-fixed) are individually interpretable in conservation-relevant terms:

- Biogenic salt redistributes equatorial precipitation toward the winter-ward hemisphere — rain rises by +0.62 mm/day at 5°S and falls by -0.31 mm/day at 5°N in the April simulation — a measurable change in the tropical water cycle that affects river systems, forest ecosystems, and regional agriculture in the Amazon, Congo, and Southeast Asian basins.
- Antarctica cools by -1.26 K when salt is present in the hemisphere entering its winter season. This is about one third of the total Antarctic warming signal since pre-industrial

times — a large enough magnitude that deforestation-driven salt removal could plausibly be contributing to observed polar change.

- Southward poleward moisture transport at 30°S is reduced by -61 TW when salt is present, supporting the moisture-barrier interpretation in the winter-ward hemisphere.

Trees are not just carbon sinks. They appear to be **active climate regulators** that modulate where on Earth latent heat is deposited. Removing rainforests removes not only a carbon reservoir but a biogenic aerosol source whose influence on the global atmospheric circulation may be substantial, variable, and currently unmodeled. The direction of that influence — whether salt increases or decreases polar heating on net, and with what regional pattern — is what we need the climate modeling community to help us determine.

Replanting and protecting equatorial rainforests would preserve whatever this mechanism does. If the current April 240 km indication of Antarctic cooling generalizes, rainforest preservation helps protect the winter pole. If the variance-amplifier hypothesis is confirmed, rainforests preserve a stabilizing influence on otherwise chaotic heat redistribution. If neither holds, we still learn something important about biosphere-atmosphere coupling that climate models currently ignore.

The polar bear and the emperor penguin may depend on many things we don't yet understand about the atmospheric effects of equatorial forests. The sensitivity we have demonstrated is sufficient reason, regardless of the specific direction of effect, to ensure that forests are not removed faster than we can understand what we are losing.

Author Background

The author is an independent researcher with an engineering and numerical-modeling background (graduate training in thermofluids, plasma physics, and two-phase flow; patents in semiconductor processing, plasma physics, and microbiome research). This work was conducted outside formal atmospheric-science institutions and is offered as an open, testable hypothesis.

Acknowledgments

This work used extensive AI coding and reasoning assistance. Claude Code (Anthropic) handled Docker container construction, MPAS compilation, Fortran modifications for the GCCN tracer, experiment orchestration, and analysis scripts. ChatGPT (OpenAI) provided an independent equation-verification cross-check during the derivation of the microphysics, which identified three errors in the original equations (terminal-velocity approximation, microphysics pathway assignment, and the critical supersaturation for ammonium sulfate) that were subsequently corrected.

The human author is responsible for all scientific claims, interpretations, and limitations. AI tools performed execution and cross-verification; scientific judgment was retained by the author.

We thank the MPAS-Atmosphere development team at NCAR and LANL for the open-source atmospheric modeling framework; NOAA for the GFS initial conditions; the WRF/WPS team for preprocessing tools; and the open-source scientific Python community (NumPy, netCDF4, Matplotlib, Cartopy) for analysis tools. This research was self-funded.

References

1. Twomey, S. (1977). The influence of pollution on the shortwave albedo of clouds. *Journal of the Atmospheric Sciences*, 34, 1149–1152.
2. Albrecht, B. A. (1989). Aerosols, cloud microphysics, and fractional cloudiness. *Science*, 245(4923), 1227–1230.
3. Rosenfeld, D. (2000). Suppression of rain and snow by urban and industrial air pollution. *Science*, 287(5459), 1793–1796.
4. Andreae, M. O., Rosenfeld, D., Artaxo, P., Costa, A. A., Frank, G. P., Longo, K. M., & Silva-Dias, M. A. F. (2004). Smoking rain clouds over the Amazon. *Science*, 303(5662), 1337–1342.
5. Rosenfeld, D., et al. (2008). Flood or drought: How do aerosols affect precipitation? *Science*, 321(5894), 1309–1313.
6. Stevens, B., & Feingold, G. (2009). Untangling aerosol effects on clouds and precipitation in a buffered system. *Nature*, 461, 607–613.

7. Gunthe, S. S., et al. (2009). Cloud condensation nuclei in pristine tropical rainforest air of Amazonia: size-resolved measurements and modeling of atmospheric aerosol composition and CCN activity. *Atmospheric Chemistry and Physics*, 9, 7551–7575.
8. Martin, S. T., et al. (2010). Sources and properties of Amazonian aerosol particles. *Reviews of Geophysics*, 48, RG2002.
9. Pöschl, U., et al. (2010). Rainforest aerosols as biogenic nuclei of clouds and precipitation in the Amazon. *Science*, 329(5998), 1513–1516.
10. Pöhlker, C., et al. (2012). Biogenic potassium salt particles as seeds for secondary organic aerosol in the Amazon. *Science*, 337(6098), 1075–1078.
11. Tao, W.-K., Chen, J.-P., Li, Z., Wang, C., & Zhang, C. (2012). Impact of aerosols on convective clouds and precipitation. *Reviews of Geophysics*, 50, RG2001.
12. Artaxo, P., et al. (2013). Atmospheric aerosols in Amazonia and land use change: from natural biogenic to biomass burning conditions. *Faraday Discussions*, 165, 203–235.
13. Thompson, G., & Eidhammer, T. (2014). A study of aerosol impacts on clouds and precipitation development in a large winter cyclone. *Journal of the Atmospheric Sciences*, 71, 3636–3658.
14. Koren, I., Dagan, G., & Altaratz, O. (2014). From aerosol-limited to invigoration of warm convective clouds. *Science*, 344(6188), 1143–1146.
15. Martin, S. T., et al. (2016). The Green Ocean Amazon Experiment (GoAmazon2014/5) observes pollution affecting gases, aerosols, clouds, and rainfall over the rain forest. *Bulletin of the American Meteorological Society*, 98(5), 981–997.
16. Berry, E. X., & Reinhardt, R. L. (1974). An analysis of cloud drop growth by collection. *Journal of the Atmospheric Sciences*, 31, 1814–1831.
17. Jensen, J. B., & Lee, S. (2008). Giant sea-salt aerosols and warm rain formation in marine stratocumulus. *Journal of the Atmospheric Sciences*, 65, 3678–3694.
18. Skamarock, W. C., et al. (2012). A multiscale nonhydrostatic atmospheric model using centroidal Voronoi tessellations and C-grid staggering. *Monthly Weather Review*, 140, 3090–3105.

Computational Details

All simulations were performed on a consumer laptop (Intel i7-12700H, 20 threads, 64 GB RAM) using Docker containers. MPAS v7.0 was compiled inside a CentOS 7 container with gfortran 8, OpenMPI 4.0, NetCDF 4.6.2, and PIO 2.6.2. MPAS v8.3.1 (including prognostic aerosol transport and the GCCN tracer modification) was compiled inside an Ubuntu 22.04 container with gfortran 11, OpenMPI 4.1, and NetCDF 4.9. Each 30-day global simulation

required approximately 1.5–2.5 hours of wall time on 12 MPI processes. A total of 12 paired simulations were completed across six experimental phases.

Appendix A: GCCN Salt Microphysics — Derivations and Calculations

This appendix presents the complete set of equations used to model Giant Cloud Condensation Nuclei (GCCN) from biogenic salt aerosols. All equations were derived from published literature and cross-verified with OpenAI ChatGPT, which identified and corrected three errors in the original derivations.

A.1 Kappa-Köhler Activation Theory

Source: Petters, M. D. and Kreidenweis, S. M. (2007), *Atmospheric Chemistry and Physics*, 7, 1961–1971.

Note on electrical neutrality. The formulation below is the standard **neutral** κ -Köhler equation — it contains no charge term, no Coulomb cross-section, no Debye length. Charged-aerosol Köhler variants exist (e.g., Jones & Sparks 1992) and reduce to this equation in the limit of particle charge $Q \rightarrow 0$. We adopt the neutral form as our starting point because airborne cloud CCN are approximately electrically neutral in bulk, and any charge correction is second-order for the activation supersaturations of interest here.

The critical supersaturation at which a dry aerosol particle of diameter D_d and hygroscopicity parameter κ activates as a cloud droplet:

$$s_{\text{crit}} = \sqrt{\frac{4 A^3}{27 \kappa D_d^3}}$$

where the Kelvin curvature parameter A is:

$$A = \frac{4 \sigma_w M_w}{R T \rho_w}$$

with constants:

SYMBOL	VALUE	DESCRIPTION
σ_w	0.072 J/m ²	Surface tension of water at ~298 K
M_w	0.018015 kg/mol	Molecular weight of water
R	8.314 J/(mol·K)	Universal gas constant
ρ_w	997 kg/m ³	Density of water

Evaluation at $T = 298$ K:

$$A = \frac{4 \times 0.072 \times 0.018015}{8.314 \times 298 \times 997} = \frac{0.00519}{2,469,832} = 2.1 \times 10^{-9} \text{ m}$$

Hygroscopicity parameters κ :

SUBSTANCE	K	SOURCE
NaCl (sea/tree salt)	1.28	Petters & Kreidenweis 2007
KCl (tree fungal salt)	0.99	Derived from thermodynamics
(NH ₄) ₂ SO ₄ (pollution)	0.61	Petters & Kreidenweis 2007
Secondary organic aerosol	0.1–0.3	Various
Black carbon (soot)	~0.0	Hydrophobic

Example: Tree salt (2 μm dry KCl, $\kappa = 0.99$):

$$s_{\text{crit}} = \sqrt{\frac{4 \times (2.1 \times 10^{-9})^3}{27 \times 0.99 \times (2.0 \times 10^{-6})^3}} = \sqrt{\frac{3.70 \times 10^{-26}}{2.14 \times 10^{-16}}} = \sqrt{1.73 \times 10^{-10}} = \mathbf{0.0013\%}$$

Comparison: Pollution aerosol (0.1 μm (NH₄)₂SO₄, $\kappa = 0.61$):

$$s_{\text{crit}} = \sqrt{\frac{4 \times (2.1 \times 10^{-9})^3}{27 \times 0.61 \times (1.0 \times 10^{-7})^3}} = \sqrt{\frac{3.70 \times 10^{-26}}{1.65 \times 10^{-20}}} = \sqrt{2.25 \times 10^{-6}} = \mathbf{0.15\%}$$

(Corrected from initial estimate of 0.3% after ChatGPT verification.)

Salt GCCN activates **115× more easily** than pollution aerosol. This is the fundamental chemical difference that drives the hypothesis.

A.2 Collision-Coalescence Efficiency

Source: Hall, W. D. (1980), *J. Atmos. Sci.*, 37, 2486–2507.

The gravitational collision efficiency $E(R, r)$ between a collector drop of radius R and a collected droplet of radius r :

R (MM)	R (MM)	E	SIGNIFICANCE
20	10	0.02	The “coalescence gap” — nearly zero
30	10	0.1	Collection barely begins
40	10	0.4	Growing efficiency
50	10	0.6	GCCN-activated drop size
60	10	0.8	Efficient collection
100	10	0.9	Rain-sized collector

The coalescence gap ($E \approx 0$ for $R < 20 \mu\text{m}$) is why autoconversion is slow ($\sim 17\text{--}24$ min). A single GCCN-activated drop at $50 \mu\text{m}$ bypasses this gap with $E = 0.6$, producing rain in ~ 5 min.

A.3 Terminal Velocity

Source: Beard, K. V. (1976), *J. Atmos. Sci.*, 33, 851–864.

Stokes law for a $50 \mu\text{m}$ radius water drop:

$$V_{\text{Stokes}} = \frac{2}{9} \frac{\rho_w g R^2}{\mu_{\text{air}}} = \frac{2}{9} \frac{997 \times 9.81 \times (50 \times 10^{-6})^2}{1.8 \times 10^{-5}} = 0.30 \text{ m/s}$$

Reynolds number check:

$$\text{Re} = \frac{2 \rho_{\text{air}} V R}{\mu_{\text{air}}} = \frac{2 \times 1.2 \times 0.30 \times 50 \times 10^{-6}}{1.8 \times 10^{-5}} = 2.0$$

Stokes law is valid for $Re \ll 1$. At $Re = 2$, a correction is needed. The model implements a size-dependent lookup based on Beard (1976):

R (MM)	V (M/S)	NOTES
<20	0	Too small for gravitational settling to matter
20–40	0.12	Small drop regime
40–60	0.25	Beard 1976 empirical ($Re \approx 2$)
>60	0.50	Large drop regime

(Stokes overestimates by 15–20% at 50 μm . Corrected after ChatGPT verification.)

A.4 GCCN Collection Rate

The continuous collection equation for GCCN drops collecting cloud water:

$$\left. \frac{dq_r}{dt} \right|_{\text{GCCN}} = \pi R(t)^2 V(R) E(R) q_c N_{\text{GCCN}}$$

where $R(t)$, $V(R)$, and $E(R)$ are all **size-dependent** — they evolve as the GCCN drop grows by condensation each timestep:

SYMBOL	VALUE	DESCRIPTION
$R(t)$	10–100 μm	GCCN drop radius, grows via condensation
$V(R)$	0–0.50 m/s	Terminal velocity (Beard 1976), size-dependent
$E(R)$	0–0.80	Collision efficiency (Hall 1980), size-dependent
q_c	variable	Cloud water mixing ratio (kg/kg)
N_{GCCN}	variable	GCCN number concentration from tracer ($\#/m^3$)

The size-dependent lookup tables implemented in the model:

R (MM)	V (M/S)	E	COLLECTION RATE RELATIVE TO $R=50$
<20	0	0	0 (coalescence gap)
20–30	0.12	0.05	0.01×
30–40	0.12	0.20	0.06×
40–50	0.25	0.50	0.53×
50–70	0.25	0.65	1.0× (reference)
>70	0.50	0.80	4.9×

A freshly activated GCCN at 10 μm collects *nothing* — it must first grow by condensation through the coalescence gap. Once it reaches ~ 40 μm , collection begins. Above 70 μm , the collection rate is nearly 5× higher than at 50 μm due to the combined increase in R^2 , V , and E .

Units derivation: The mixing ratio q_c (kg/kg) times air density ρ gives mass concentration (kg/m³). The collection kernel $\pi R^2 V E$ has units m³/s. Multiplied by N_{GCCN} (#/m³) and $q_c \rho$ (kg/m³), then divided by ρ to return to mixing ratio: the ρ factors cancel, yielding the simple form above in kg/(kg·s). (*Verified by ChatGPT.*)

Numerical example at $R = 50$ μm in a tropical cloud ($q_c = 0.5 \times 10^{-3}$ kg/kg, $N_{\text{GCCN}} = 3 \times 10^6$ m⁻³):

$$\frac{dq_r}{dt} = \pi \times (50 \times 10^{-6})^2 \times 0.25 \times 0.65 \times 0.5 \times 10^{-3} \times 3 \times 10^6 = 1.92 \times 10^{-6} \text{ kg/kg/s}$$

Cloud water lifetime under GCCN collection:

$$\tau = \frac{q_c}{dq_r/dt} = \frac{0.5 \times 10^{-3}}{1.92 \times 10^{-6}} = 260 \text{ s} \approx \mathbf{4.3 \text{ minutes}}$$

Compare with autoconversion alone: **17–24 minutes**. GCCN accelerates rain formation by a factor of 4–6×. At $R = 80$ μm (after further growth), $\tau \approx 53$ s — nearly instantaneous rain formation.

A.5 Condensational Growth

After activation, GCCN drops grow by vapor condensation (Rogers & Yau, eq. 7.18):

$$\frac{dR}{dt} = \frac{G \cdot s}{R}$$

where $G \approx 10^{-10}$ m²/s is the condensation growth parameter and s is the supersaturation. Integrating over one timestep Δt :

$$R(t + \Delta t) = \sqrt{R(t)^2 + 2 G s \Delta t}$$

Starting from $R = 10$ μm (just activated) with $s = 0.003$ (0.3%) and $\Delta t = 90$ s:

$$R = \sqrt{(10 \times 10^{-6})^2 + 2 \times 10^{-10} \times 0.003 \times 90} = \sqrt{10^{-10} + 5.4 \times 10^{-11}} \approx 12.4 \mu\text{m}$$

Growth to the efficient collection size of 50 μm requires multiple timesteps (~5–10 minutes), during which the drop continuously sweeps up cloud water.

A.6 Integration into Thompson Microphysics

Key decision (corrected after ChatGPT review): GCCN collection is added to the **accretion pathway** (`prc\rcw`), NOT the autoconversion pathway (`prc\wau`).

- **Autoconversion** (`prc\wau`): spontaneous self-collection of similarly-sized cloud droplets (Berry & Reinhardt 1974).
- **Accretion** (`prc\rcw`): large drops collecting small droplets — physically what GCCN drops do.

The full GCCN lifecycle in each microphysics timestep proceeds as follows:

1. **Activation check:** Compute s_{crit} from kappa-Köhler at the local temperature. If cloud water exists (ambient supersaturation $> s_{\text{crit}}$), all GCCN activate. For 200 nm KCl, this threshold is ~0.02%, trivially exceeded in any cloud.
2. **Condensational growth:** Grow the drop from $R = 10$ μm via $R \leftarrow \sqrt{R^2 + 2G \cdot s \cdot \Delta t}$, capped at 100 μm .
3. **Look up $V(R)$ and $E(R)$:** Terminal velocity and collision efficiency from size-dependent tables (Beard 1976, Hall 1980).
4. **Compute collection rate:** `prc\gccn` = $\pi R^2 V E \cdot q_c \cdot N_{\text{GCCN}}$, limited by available cloud water.

5. **Add to accretion:** $\text{pr}\text{r}\backslash\text{rcw} \leftarrow \text{pr}\text{r}\backslash\text{rcw} + \text{pr}\text{r}\backslash\text{gccn}$.
6. **Update cloud droplet number:** Droplets collected by GCCN are removed from $\text{pnc}\backslash\text{rcw}$.
7. **Update rain drop number:** GCCN drops that grew past D_{0r} add to $\text{pnr}\backslash\text{wau}$.
8. **Wet scavenging:** In sub-cloud layers where rain exists, unactivated GCCN particles are swept out by falling rain drops using the Thompson $\text{Eff}\backslash\text{aero}$ function with the 200 nm salt particle size. This depletes ngccn1d in proportion to the rain rate, the aerosol collection efficiency, and the rain drop size distribution.

A.7 Observed Precipitation Enhancement from Salt Seeding

EXPERIMENT	METHOD	ENHANCEMENT	SOURCE
South Africa	Hygroscopic flares	30–60%	Mather et al. 1997
India (CAIPEEX)	Salt seeding	28% (95% conf.)	BAMS 2023
Salt powder model	Convective clouds	2–3× rain flux	Selvakumar et al. 2010
Optimal particle size	Milled salt powder	100× vs flares	Rosenfeld et al. 2010

A.8 Corrections Identified by Cross-Verification

#	ORIGINAL ERROR	CORRECTION	IMPACT
1	$V = 0.30$ m/s (Stokes)	$V = 0.25$ m/s (Beard 1976)	15–20% overestimate of collection
2	Added to $\text{pr}\text{r}\backslash\text{wau}$ (autoconversion)	Added to $\text{pr}\text{r}\backslash\text{rcw}$ (accretion)	Wrong physical pathway
3	$s_{\text{crit}} = 0.3\%$ for $(\text{NH}_4)_2\text{SO}_4$	$s_{\text{crit}} = 0.15\%$	Factor of 2 error in baseline

This cross-verification demonstrates the value of using multiple AI systems: one derives and implements, the other verifies independently. We recommend this practice for all computational research.

Appendix B: Origin of the Idea

This appendix preserves the informal development-history narrative of how the hypothesis was first conceived. It is not part of the formal scientific argument — readers focused on methods and results can skip it.

The hypothesis originated from a simple observation on a weather map displayed on an iPhone: equatorial rainforests showed *continuous* rainfall while the adjacent oceans showed *intermittent* rainfall. This seemed backwards. Oceans have unlimited water for evaporation —why would rain be more persistent over land?

A mental model formed through several steps. First, the evaporative surfaces of leaves and the active metabolic pumping of water by trees could explain enhanced local humidity. But tropical rainforest topsoil is shockingly thin—typically 9–15 inches—far too shallow to store significant water. Trees in this environment must receive nearly continuous rain or mist, or they die. One possible ecohydrological interpretation is that traits which help trees secure a reliable local water supply could be selectively favored.

This led to a question: *might rainforest tree ecosystems be emitting something that influences cloud formation overhead?* A search of the cloud-seeding literature for biogenic sources turned up Pöhlker et al. (2012), a study led by researchers at the Max Planck Institute for Chemistry (Mainz, Germany) with Lawrence Berkeley National Laboratory collaborators who performed the electron microscopy. They demonstrated that fungi associated with Amazon rainforest trees eject potassium salt nanoparticles that can serve as cloud condensation nuclei, seeding local cloud formation and precipitation. The rainforest–fungal aerosol system may therefore act, in effect, as a continuous distributed source of warm-rain nuclei above the emitting canopy — loosely analogous to the airplanes used for cloud-seeding programs in drier regions.

The next insight came from thermodynamics. If salt controls where condensation occurs, it also controls where **latent heat** is released. Every gram of water vapor that condenses releases 2,500 joules of heat into the surrounding air. Where the rain goes, the heat goes. The atmosphere functions as a **heat pipe**—water vapor carries latent energy from the

surface to the altitude and location where it condenses, depositing that energy as sensible heat.

If salt traps rain locally at the equator, it traps heat at the equator. If the forests are cut and the salt source is removed, that humidity is free to travel poleward, carrying its latent heat with it and releasing it closer to the poles. This is not a greenhouse gas mechanism—it does not change how much heat Earth traps from the sun. It is a **redistribution** of heat by convection: changing where existing thermal energy is deposited.

An analogy from everyday experience makes the magnitude intuitive: ice cubes in a glass of water melt slowly when the water is still, because a cold thermal boundary layer forms around the ice and insulates it. Stir the water and the ice melts dramatically faster—not because stirring adds significant energy, but because it thins the thermal boundary layer, steepening the temperature gradient and allowing heat to conduct to the ice surface faster. The energy from stirring is negligible compared to the thermal energy already in the water; the stirring merely **redistributes** it more efficiently. Similarly, removing the equatorial salt barrier does not add heat to the climate system—it stirs the existing latent heat poleward more efficiently, thinning the thermal stratification that kept the poles cold.

This analogy suggests the effect could be substantial. The atmosphere’s total poleward energy transport is approximately 5 petawatts. Even a few percent change in this transport—driven by the loss of the equatorial moisture barrier—could deliver enough extra heat to significantly accelerate polar ice loss.